Environmental Science Nano

A multi-nutrient nanocomposite enhances UV stress tolerance and modulates nutrient accumulation in lettuce

Journal:	*Environmental Science: Nano*
Manuscript ID	EN-ART-02-2025-000154.R1
Article Type:	Paper

Environmental Significance Statement

The increasing intensity of ultraviolet (UV) radiation due to climate change poses a significant challenge to crop productivity and food security. This study presents a multinutrient nanocomposite designed for dual functionality—protecting plants from UV-induced stress while enhancing nutrient accumulation. The controlled release of Mg, Mn, Zn, and Fe improves plant resilience, reducing oxidative stress and promoting sustainable growth. By integrating nanotechnology with plant physiology, this work offers a sustainable, nanoenabled agricultural strategy to mitigate UV stress while enhancing nutrient use efficiency. These findings contribute to environmentally friendly solutions for improving crop resilience in the face of climate stressors.

A multi-nutrient nanocomposite enhances UV stress tolerance and modulates nutrient accumulation in lettuce

Raja muthuramalingam Thangavelu, *[a] Washington da Silva, [a] Jose A. Hernandez-Viezcas,[b] Vinka Oyanedel-Craver,[c] Jorge L. Gardea-Torresdey,[bd] Christian O. Dimkpa, [a] Jason C. White, [a] and Nubia Zuverza Mena.*[a]

a. Connecticut Agricultural Experiment Station, New Haven, CT 06511, United States.

b. Department of Chemistry and Biochemistry, The University of Texas at El Paso, 500 West University Avenue, El Paso, TX 79968, USA

c. Department of Civil and Environmental Engineering, University of Rhode Island, Kingston, RI, USA

d. Environmental Science and Engineering PhD Program, University of Texas at El Paso, El Paso, USA

*Corresponding authors:Nubia.zuverza@ct.gov and raja.muthuramalingam@ct.gov

Abstract

This study introduces a novel multielement (Zn-Mg-Mn-Fe) nanocomposite that serves both as a UV-protective agent and a nutrient delivery system for *Lactuca sativa* (lettuce). Plants were grown indoors in a potting soil-like mix, under artificial lighting (from light emitting diodes, LEDs) or under LED+UV radiation to simulate excessive sunlight exposure (light stress). Lettuce was treated with foliar applications of the nanocomposite at 100 mg/L, 200 mg/L, and 300 mg/L, with 1 mL applied per plant during the fifth week of growth (a total of 0.1, 0.2 or 0.3 mg of the composite respectively per plant). Plants were exposed to UV radiation (360–400 nm) for 10 hours daily over two weeks. The 300 mg/L treatment significantly enhanced photosynthetic efficiency and plant growth, increasing chlorophyll content (66.7% ± 3.5), leaf area (45% ± 2.1), and dry biomass (43.68% ± 1.8) compared to untreated and ionic controls. It also mitigated UV-induced stress, reducing UV-induced damage scores by 73% compared to controls and lowering stress markers, with flavonoid production reduced to 30.5% ± 2.3 of control levels and SOD activity reduced to 25.8% ± 1.8 of control levels. The composite's-controlled nutrient release mechanism facilitated rapid Mg uptake (220 mg/kg dry weight in leaves within 4 days) and sustained delivery of Zn, Mn, and Fe over a 7–10-day period. Long-term nutrient uptake analysis showed increases in Mn (55.3% ± 3.2), Mg (47.8% ± 2.7), and Fe (62.5% ± 4.1). Enhanced P (28.5% ± 2.2) and K (35.7% ± 3.1) accumulation further boosted the nutritional quality of edible tissues. Additionally, the nanocomposite demonstrated the unique ability to convert harmful UV radiation into visible light, providing dual benefits of UV protection and enhanced photosynthetic activity. These findings highlight the potential of this multi-functional nanocomposite as a sustainable solution to improve crop resilience, optimize nutrient delivery, and combat environmental stress in agricultural systems.

Keywords

UV-stress mitigation, nano-sunscreen, nano-Zn-Mg-Mn-Fe composite, nutrient delivery system, photosynthetic efficiency

1. Introduction

Innovations in agricultural practices, particularly in plant nutrition and fertilization, continue to focus on maximizing crop yields, improving plant health, and mitigating environmental stress. (1),(2) One significant global challenge is the rising temperature and increased UV radiation exposure caused by climate change and ozone layer depletion resulting from anthropogenic activities.(3) Agricultural regions in tropical and subtropical zones are especially vulnerable due to their higher solar exposure and extended growing seasons. For example, UV-B radiation has increased by 6–14% at mid- and high-latitude agricultural regions since the 1980s, with some areas experiencing ozone-related UV-B increases of up to 20%.(4) The depletion of the ozone layer has led to elevated levels of solar UV radiation reaching the Earth's surface, notably UV-B (280–315 nm) and UV-A (315–400 nm), while UV-C (100–280 nm) remains completely absorbed by the atmosphere.(5) UV-B radiation, which partially penetrates the atmosphere, has harmful effects on plants, including reduced photosynthesis, impaired growth, and lower crop yields. For instance, increased UV-B exposure has been shown to reduce wheat yield by 20–30% and impair dry matter accumulation in maize.(6,7) UV-A radiation reaches the surface largely unfiltered, contributing to long-term oxidative stress in plants. Compounding this issue, climate-related factors such as wildfire smoke and increased atmospheric aerosols can modulate UV radiation levels by reducing its penetration, underscoring the complexity and variability of these challenges under shifting environmental conditions. This enhanced exposure to UV radiation can cause extensive damage to DNA,

proteins, lipids, and cellular membranes in biota, posing significant biological and environmental challenges, particularly for crop productivity and food security.(8–10)

Plants, being stationary and reliant on sunlight for photosynthesis, are particularly vulnerable to increased UV-B and UV-A exposure.(11,12) While UV radiation plays a role in regulating photomorphogenesis by inhibiting hypocotyl elongation, promoting cotyledon expansion, and inducing flavonoid accumulation, excessive UV exposure can severely harm plants by damaging DNA, increasing the production of reactive oxygen species (ROS) that cause oxidative stress and damage, and impairing photosynthesis.(13–16) Plants have evolved adaptive mechanisms to cope with UV-induced stress, such as synthesizing UV-absorbing compounds like flavonoids, anthocyanins, and phenolic acids, and modifying physiological pathways to mitigate damage and maintain growth.(17,18) However, these innate defences are often insufficient to combat severe UV damage.(5,19)Additionally, UV radiation can alter the chemical composition of plants, influencing their interactions with herbivores and pollinators and potentially disrupting ecological balance. In response to UV stress, many plants enhance the production of secondary metabolites, including phenolic compounds and flavonoids.(11) Given their protective roles, the potential toxic effects of excessive flavonoid accumulation are often overlooked. At high concentrations, flavonoids may act as mutagens, pro-oxidants that generate free radicals, or inhibitors of critical enzymes involved in hormone metabolism.(20)

Innovative solutions to mitigate the negative impacts of increasing UV radiation are urgently needed. While addressing the root cause remains a long-term goal, strategies are being developed to protect plants from harmful UV rays, mirroring the way sunscreens shield humans. Zinc oxide and titanium dioxide (TiO_2), widely used in sunscreens,(21) are well-recognized for their UV shielding properties, along with organic chemical counterparts such as oxybenzone, ensulizole, and ethylhexyl salicylate.(22) To address the dual challenge of protecting plants from harmful UV radiation and enhancing their physiological performance,

we developed a multifunctional nanocomposite incorporating zinc (Zn), magnesium (Mg), manganese (Mn), and iron (Fe). Zinc was selected as the core component due to its well-documented ability to absorb and scatter UV radiation, making it an effective shielding agent. Magnesium, manganese, and iron were intentionally integrated for their essential roles in plant metabolism: Mg is central to chlorophyll structure and photosynthetic efficiency; Mn acts as a cofactor in the oxygen-evolving complex of photosystem II and supports antioxidant defense;(23) Fe is crucial for electron transport, enzyme function, and redox balance.(23) The nanoscale formulation enhances the surface area and reactivity of these elements, allowing for improved foliar adhesion, controlled release, and efficient uptake. This rationale underpins our design of a composite material that synergistically combines UV protection with targeted nutrient delivery, offering a novel approach to improving crop resilience under stress conditions. We hypothesize that the foliar spraying of this nano-Zn-Mg-Mn-Ferrite composite will provide protection against UV irradiation, enhance photosynthetic efficiency, and improve nutrient uptake and delivery in plants, promoting optimal growth and productivity under radiation stress.

More specifically, the nano-Zn-Mg-Mn-Fe composite represents an innovative approach to foliar spraying, harnessing the synergistic effects of Mn-, Fe-, Mg-, and Zn-based compound at the nanoscale. These elements play critical roles in photosynthetic processes such as chlorophyll synthesis, electron transport, and water splitting.(24–28) Zinc is also included to enhance plant micronutrition as part of an agronomic fortification strategy. This nanocomposite structure maximizes the bioavailability and efficacy of these micronutrients, improving both plant photosynthesis and resilience to environmental stress such as UV radiation. Foliar spraying, which involves directly applying nutrient-rich solutions onto plant leaves, has emerged as a powerful tool for boosting plant nutrition and physiology, as well as generating climate resilience.(23,29) This work adds to a rapidly growing body of evidence demonstrating

the unique and highly beneficial impacts of nanoscale nutrients on crop growth and resilience, and significantly expands the tool box for developing sustainable nano-enabled agriculture in a changing climate.

2. Materials and methods

2.1 Materials

All chemicals used in this study including zinc sulfate, magnesium sulfate, iron (III) sulfate, manganous sulfate, and potassium hydroxide (KOH) were of analytical or reagent grade with the highest available purity and were purchased from Sigma-Aldrich and Merck Millipore. Ultrapure Milli-Q (Millipore-18m Ω cm^{-1}) water was used for the reagent preparation, nanocomposite and ionic mixture dilution, and other experimental work. Glassware used for the nanoparticle processing were initially rinsed with *aqua regia* (3 parts HCl to one-part HNO_3) and thoroughly washed three times with Milli-Q, then oven-dried before use. Lights were purchased from Medic Grow, specifically the Spectrum Y Wireless LED Grow Light 880W with tunable full spectrum. The product comes with UV+IR bars by default, providing enhanced light spectrum options for optimized plant growth and stress studies.

Synthesis and characteristics of nano-Zn-Mg-Mn-Ferrite composite

The nano-Zn-Mg-Mn-ferrite composite was synthesized using the co-precipitation method. Zinc sulfate (200 mM), magnesium sulfate (100 mM), iron (III) sulfate (100 mM), and manganous sulfate (100 mM) were mixed in a stoichiometric ratio of 2:1:1:1 and dissolved in deionized water under constant stirring at 800 rpm for 1 hour at 55°C.(30) This ratio was selected because it ensures the balanced incorporation of metal ions into the ferrite structure, optimizing the physicochemical properties necessary for UV shielding, nutrient delivery, and photosynthetic enhancement in plants. This composition directly influences the functional behavior of the nanocomposite. The nanoscale particle size (~100–200 nm) enables uniform

coverage on the plant leaf surface, which is critical for consistent UV protection. The metal oxides present in the composite Zn, Mg, Mn, and Fe exhibit wide band gaps and high refractive indices, contributing to strong UV absorption and scattering, particularly in the UV-A and UV-B spectrum. Moreover, the surface charge (moderately negative zeta potential) enhances colloidal stability and promotes strong adhesion to the hydrophilic leaf surface, reducing particle runoff and ensuring prolonged retention. These physicochemical attributes work synergistically to form an effective foliar sunscreen that shields plant tissues from UV-induced damage while simultaneously facilitating micronutrient delivery. To the solution, 5M KOH was added dropwise until the pH reached 10-11 while maintaining stirring conditions at 800 rpm at 50°C. The solution's color was monitored, with a transition from golden orange to dark brown indicating the formation of the ferrite precipitates. The mixture was stirred continuously until the precipitation process was complete, yielding the desired nano-ferrite composite. The final nano-Zn-Mg-Mn-ferrite composite was washed twice by centrifugation using deionized water, thoroughly dried at 60°C, and then ground into a fine powder with a ceramic mortar and pestle. The chemical reactions involved are the precipitation of metal hydroxides followed by their transformation into the ferrite structure.

A simplified reaction equation for the synthesis is as follows:

$$\mathbf{2\ ZnSO_4 + MgSO_4 + Fe_2(SO_4)_3 + MnSO_4 + 14\ KOH \rightarrow Zn_2MgMnFe_2O_4 + 7\ K_2SO_4 + 7\ H_2O}$$

This co-precipitation method was selected to ensure the balanced incorporation of metal ions into the ferrite structure, optimizing the physicochemical properties essential for UV shielding, nutrient delivery, and photosynthetic enhancement in plants.

2.2.1 Nanomaterial characterization

The synthesized material underwent thorough characterization to evaluate nanoscale properties and ensure uniformity throughout different stages of the process. A Transmission Electron Microscopy (TEM, Hitachi HT7800) was employed to visually assess the morphology and size of the particles. Dynamic Light Scattering (DLS) analysis using a Malvern Zetasizer Ultra was performed to measure the hydrodynamic diameter of the particles (1 mg dispersed in 5 mL of deionized water, pH.7.2, and ultrasonicated). The results confirmed that the particles remained within the desired nanoscale range of 10-50 nm. Images obtained from TEM were also used to determine the particle size distribution using ImageJ, a Java-based image processing program. Zeta potential (ζ) analysis was performed to evaluate the surface charge and dispersion stability of the nanoparticles. For the measurement, 1 mg of nanoparticles was dispersed in 5 mL of deionized water, adjusted to pH 6.5, and ultrasonicated. The ionic strength of the medium was maintained at approximately 1 mM using KCl to ensure consistent and reliable readings. After multiple iterations to optimize the synthesis process, the final molar concentrations were standardized to achieve consistency, resulting in a 2:1:1:1 ratio. X-ray Diffraction (XRD) was performed using a Rigaku SmartLab X-ray Diffractometer to determine the crystalline structure of the nanocomposite materials, providing detailed insights into their phase composition, and details to infer their oxidation states. Powdered nanocomposite samples were analyzed using both XRD and Fourier Transform Infrared Spectroscopy (FTIR) with a Bruker INVENIO-S instrument. FTIR-ATR (Attenuated Total Reflectance) was employed to identify specific functional groups on the particle surface, ensuring that the surface chemistry aligned with the intended design. Scanning Electron Microscopy (SEM) coupled with Energy Dispersive X-ray Spectroscopy (EDX), performed using a Hitachi CFE SU8230, was utilized to examine the surface morphology and determine the elemental composition of the nanocomposite. An AI model powered by ChatGPT(31), was employed to generate structural graphics of the nano-Zn-Mg-Mn-ferrite composite, offering a comprehensive visualization of its morphology and

crystallography (Figure S1). This was achieved by integrating data from TEM, Scanning Electron Microscopy (SEM), and X-ray Diffraction (XRD) patterns. As noted above, TEM provided high-resolution insights into particle size and shape, SEM detailed surface topology and nanoparticle distribution, and XRD revealed the crystalline structure and phase composition. The AI model synthesized these datasets, enabling the creation of a detailed graphical representation that effectively captured the nanocomposite's structural properties. This integration not only enhanced the interpretability of the material's characteristics but also served as a novel approach to visually present multi-dimensional experimental data. The optical properties of the materials were investigated using UV-Vis spectroscopy (SpectraMax M2, Molecular Devices). This analysis encompassed a wide range of wavelengths, evaluating absorbance, excitation, and emission characteristics to assess potential upconversion properties. Specifically, the materials' ability to convert UV light into longer wavelengths in the visible range was monitored, which is critical for UV protection.

2.3 Release and uptake kinetics of nano-Zn-Mg-Mn-Fe composite

An ionic release and uptake kinetics study was performed in vitro using the nano-Zn-Mg-Mn-Ferrite composite particles. For the "discontinuous" in vitro study, 1 mg of the composite particles was suspended in 1 mL of deionized water at neutral pH and placed on a tube rotator operating at 50 rpm. At predetermined intervals—15 min, 30 min, 1 h, 2 h, 4 h, 12 h, 48 h, 7 d, 14 d, 21 d, and 30 d—a 500 µL aliquot of the colloidal solution was collected and centrifuged at 10,000 rpm (9,800 g) for 10 minutes at room temperature. The resulting supernatant was carefully collected and stored for elemental profiling following the standard acid digestion procedure. Elemental analysis was conducted using Inductively Coupled Plasma Optical Emission Spectroscopy (ICP-OES; Thermo iCAP Pro XP Radial), providing detailed insights into the release and uptake kinetics of the composite particles. The experiment was conducted in triplicate, with data from three individual analyses for each replication. An *in planta* uptake

study was conducted using a single concentration of 300 mg/L nanocomposite, which was sprayed onto the outer leaves. Leaf samples were collected daily from the inner leaves over a period of four days from the same treated plants, with three biological replicates. The leaves were thoroughly washed with deionized water, subjected to acid digestion, and analysed using ICP-OES to measure the elements from the nanoparticles present in the leaf tissues.

2.4 Lettuce growth conditions

Lettuce plants (*Lactuca sativa*, cultivar "Chalupa Organic") were selected for this study due to their sensitivity to light and heat, as well as their broad leaf lamina, which ensures effective absorption of foliar spray treatments. Individual seeds were sown in seed starting trays filled with PRO-MIX® potting mix (pH 5.2-6.2) and germinated in a glasshouse maintained at a controlled temperature of 26-28°C. After two weeks, the seedlings were transplanted into individual 4-inch square pots filled with PRO-MIX® potting mix and moved to a walk-in growth chamber for further development. The growth chamber was maintained at 26 ± 3°C, 65% relative humidity, and a 16-hour photoperiod, ensuring optimal growth conditions in an insect-free environment. The plants were watered regularly via the trays to ensure consistent soil moisture levels. For foliar spray experiments, four-week-old plants with five to six fully developed leaves were used to ensure uniformity in treatment absorption.

2.5 Foliar application and UV exposure

Three different concentrations—100 mg/L (0.1 mg/plant), 200 mg/L (0.2 mg/plant), and 300 mg/L (0.3 mg/plant)—of both the nano Zn-Mg-Mn-ferrite composite and the cognate ionic mixture of Zn-Mg-Mn-Fe, using the same molar ratios as the nanocomposite, were prepared. Before each application, both solutions were ultrasonicated for 1 minute to maximize particle dispersion. The treatments were applied to the plants via foliar spraying using a precision atomizer (portable oxygen injector, FILFEEL, Amazon marketplace), targeting the entire leaf

abaxial and adaxial surfaces. Each plant received a maximum of 1 mL of foliar spray per treatment, applied uniformly across all treatments with 10 replicates. Foliar sprays were performed once during the 5th week of the experiment. To prevent root exposure, the containers' potting mix were covered with aluminum foil during the application. The plants were exposed to a combination of UV light and LED light (wavelength range: 360–600 nm) at 300 W for 10 hours per day for two weeks following the foliar spray application. In a separate experiment, a different group of plants was exposed exclusively to LED light to evaluate the comparative growth effects of the nano-Zn-Mg-Mn ferrite composite and its ionic mixture. Plants sprayed with DI water served as the control group for both experiments.

2.6 Final assessment

Leaf discoloration and damage, including photobleaching or chlorosis, necrosis, and other forms of visible tissue injury, were used as indicators of UV radiation damage. The extent of UV-induced damage was digitally documented near the 7th week, just before harvesting. Visible symptoms such as yellowing and leaf burn were classified into three severity levels: mild, moderate, and severe. To quantify these symptoms, a standardized rating scale ranging from 0 to 5 was applied, as detailed in Table 1.(32) Each treatment group included 10 biological replicates, and scoring was performed consistently across all replicates to ensure robust comparative analysis. Based on these scores, a heat map was generated using Origin Pro 8, a statistical software tool. The scale is defined as follows:

Score	Description
0	No visible damage
1	Slight yellowing or small areas of discoloration
2	Noticeable discoloration, slight leaf curling, or light browning at the edges
3	Moderate yellowing or browning, leaf curling, and signs of necrosis

4	Severe yellowing, browning, or necrosis on multiple leaves with significant leaf deformation
5	Complete leaf necrosis, leaf drop, or severe stunting of the plant

Prior to harvest, the photosynthetic rate and chlorophyll content were measured using various parameters indicative of plant photosynthetic efficiency (33) These parameters included SPAD (relative chlorophyll content), Phi2 (photosystem II quantum yield), PhiNPQ (quantum yield of regulated non-photochemical energy dissipation), LEF (linear electron flow), PAR (photosynthetically active radiation), NPQt (non-photochemical quenching of fluorescence), qL (fraction of open PSII reaction centers), Fo' (minimal fluorescence after dark adaptation), FmPrime (maximal fluorescence after a light pulse), and PhiNO (quantum yield of non-regulated energy dissipation). These measurements were conducted after the fifth week of growth using the MultispeQ V 2.0 device (PhotosynQ, USA), which provides non-destructive real-time, high-throughput data on plant photosynthesis and related parameters. At the end of the sixth week, the plants were harvested, and growth parameters were carefully recorded. These parameters included number of leaves, plant height, root length, leaf area, fresh biomass, and dry biomass. Fresh biomass was measured immediately after harvest, while dry biomass was determined after drying the plant samples in an oven at 60°C to a constant weight.

After harvesting, plant tissue samples were stored at -80°C for subsequent enzyme analysis to assess the activity of superoxide dismutase (SOD). The SOD activity was measured using UV-Vis spectroscopy at 560 nm. Elevated SOD activity is a key indicator of the plant's ability to manage oxidative stress, which can negatively impact photosynthesis. Additionally, the total flavonoid content in the treated plants was quantified using UV-Vis spectroscopy at optical density (OD) 510 nm. Flavonoids, as secondary metabolites, often increase in response to UV

stress in certain plant species, acting as a protective mechanism against the harmful effects of ultraviolet radiation.(13) Subsets of each sample type were oven-dried and analyzed using ICP-OES to quantify the concentrations of the applied elements (Zn, Mn, Mg, and Fe), as well as macro and secondary nutrients, including Na, K, P, S, and Ca. While Na is not considered an essential nutrient for most plants, it was included in the analysis to explore its potential role in osmotic regulation, ion balance, and interactions with other nutrients. All values are expressed in mg/kg dry weight unless otherwise stated.

2.7 Statistical analysis

Statistical analysis was performed using one-way analysis of variance (ANOVA) to evaluate the significance of differences between the treatment groups. A Tukey's post-hoc test was applied to determine specific differences between group means, with a significance threshold set at $p < 0.05$. Data are presented as mean ± standard error (SE) and depicted using box plots, with a minimum of three independent replicates and up to a maximum of 10 replicates for each treatment group. All statistical analyses were conducted using OriginPro 8 software(32), ensuring that the assumptions of normality and homogeneity of variance were met.

3. Results and Discussion

Particle Morphology and Size Distribution

Figure 1 shows the TEM analysis of the morphology and particle size of the synthesized nano-Zn-Mg-Mn-Fe composite. The images (Figures 1A and 1B) reveal a mixture of particle shapes, with regions containing both darker, spherical particles and lighter sheet-like structures. The darker areas correspond to high-density particles, likely representing the metal-rich zones within the composite, while the lighter sheet-like regions could be attributed to the presence of a matrix or support structure within the nanocomposite. The particles are well-dispersed, with no significant signs of agglomeration at either scale. Figures 1A and 1B, captured at

magnifications of 30k× and 60k× respectively, were taken at different magnifications to highlight detailed structural differences. In Figure 1A, the morphology and dispersion of the nanoparticles are evident, with the particles appearing well distributed within a sheet-like matrix. At the higher magnification (Figure 1B), finer structural details, including individual particle shapes and boundaries, become more apparent, offering a closer look at the nanoscale features of the composite. To quantify particle size, histograms were generated based on ImageJ software analysis of the TEM images.

The particle size distribution presented in Figures 1C and 1D demonstrates a relatively narrow and consistent size range, indicating uniform nanoparticle synthesis. Figure 1C (corresponding to TEM image A) shows particle sizes ranging from approximately 2 to 10 nm, with the majority of particles (over 70%) distributed between 4 and 6 nm. The mean particle diameter calculated from this distribution was approximately 4.8 ± 1.6 nm. Figure 1D (based on TEM image B) displays a slightly narrower size distribution, with particle diameters ranging from 2 to 6 nm and the majority clustered between 3 and 4 nm. The mean particle size for this group was approximately 3.2 ± 0.9 nm. These two independent analyses, derived from over 150 particles each, confirm that the synthesis method yields nanoparticles with good size uniformity and reproducibility. The narrow distribution further supports the effectiveness of the co-precipitation process in controlling particle growth, which is essential for maintaining consistent physicochemical behavior and surface reactivity. Many particle characteristics, including size, shape and crystal lattice, differ significantly from those previously reported for Zn-Mg-ferrite composites that excluded Mg, although these earlier composites were primarily generated for their magnetic properties, which were utilized for decontaminating dyes and heavy metals.(34,35) The synthesized nano-Zn-Mg-Mn-Fe composite exhibited moderate colloidal stability in aqueous dispersion, with a zeta potential of –18.7 mV and a polydispersity index (PDI) of 1, indicating a moderately uniform particle size distribution. While the

dispersion showed a tendency for slow aggregation over time, the composite demonstrated improved stability when applied to leaf surfaces. This enhanced stability is likely due to interactions with the plant cuticle, where the hydrophobic wax layer and surface microtexture help immobilize the nanoparticles, reducing their mobility and aggregation. The localized microenvironment on the leaf surface, including surface tension and humidity, contributes to maintaining particle dispersion and functional integrity. These factors collectively support the composite's sustained UV-protective performance under field-like conditions.

The presence of both small nanoparticle clusters and larger sheet-like structures could be indicative of different phases or components in the composite material. A uniform particle size distribution is important for potential applications, as it directly influences the surface area and reactivity of the nanocomposite. The TEM analysis reveals that the Zn-Mg-Mn-Fe nanocomposite consists of well-dispersed particles (PDI 1.0) embedded within sheet-like structures.

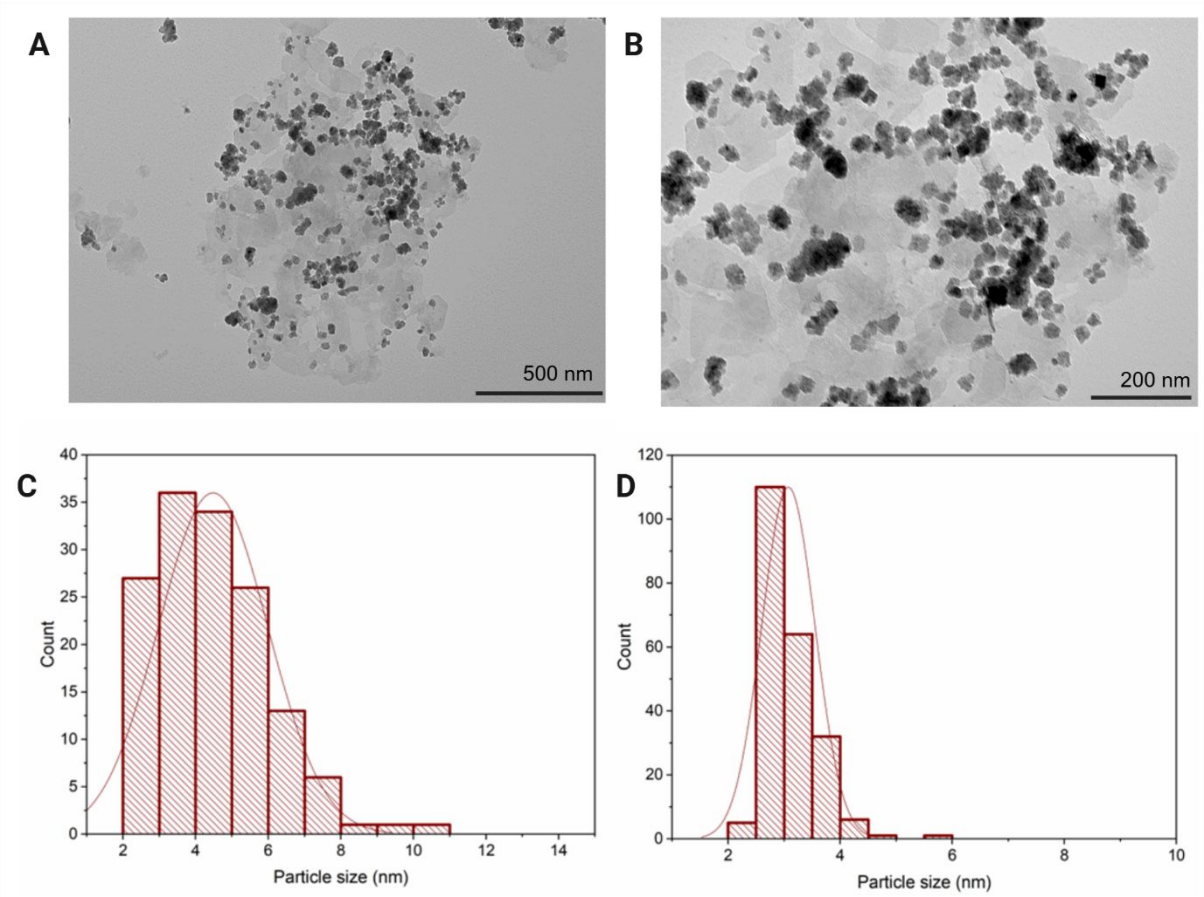

Figure 1. Transmission electron microscopy (TEM) analysis of nanocomposite particles. *(A)* TEM micrograph of the Zn-Mg-Mn-Fe nanocomposite displaying the particle morphology, including a combination of darker regions corresponding to dense particles and sheet-like structures. *(B)* TEM micrograph of the same nanocomposite imaged at a higher magnification providing a more detailed observation of the nanoparticle dispersion and morphology. *(C)* The particle size distribution histogram was generated based on measurements obtained from the TEM image, specifically focusing on the dark clusters, which represent the denser nanoparticle regions. *A)*, showing a particle size range from approximately 2 to 10 nm, with the majority of particles at 4-6 nm. *(D)* Particle size distribution histogram derived from *(B)*, illustrating a more narrowly distributed particle size range of 2 to 6 nm, with a peak at 3-4 nm. The histograms were generated using ImageJ software for particle size analysis.

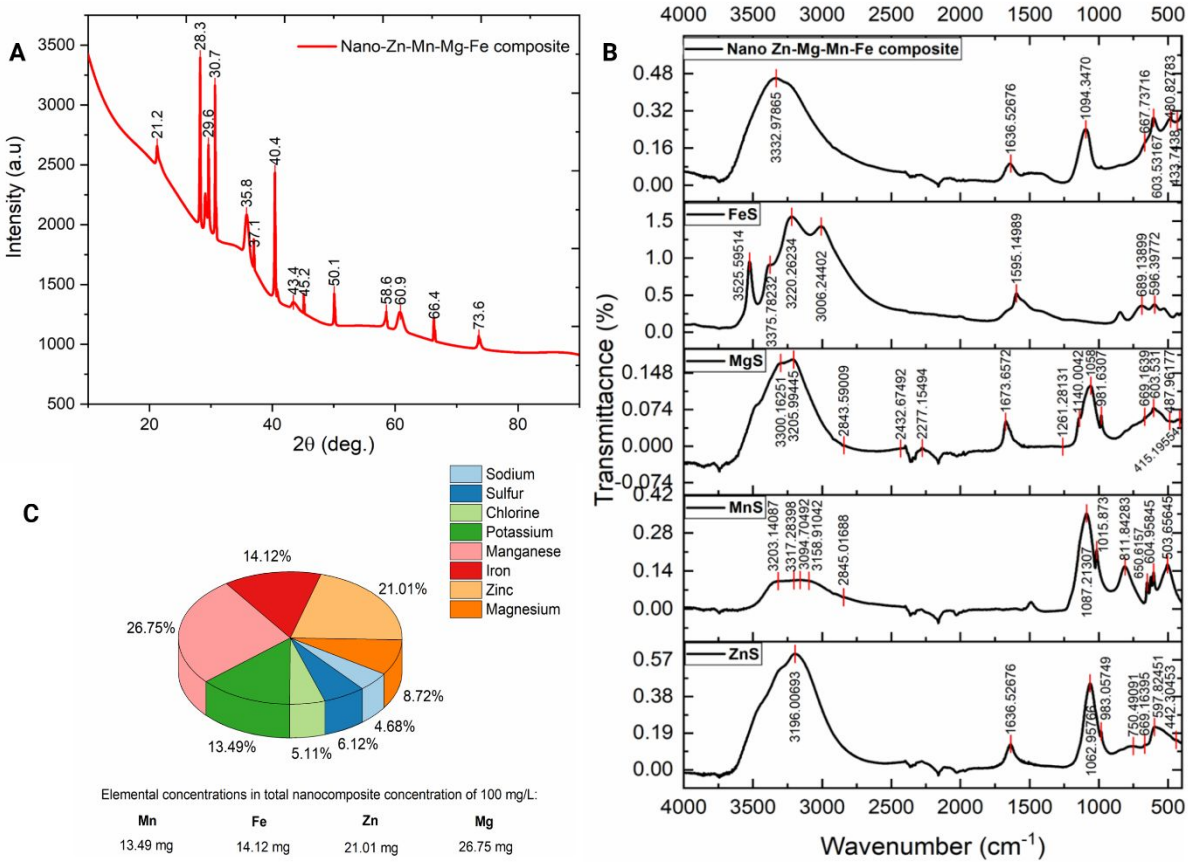

Figure 2. Characterization of the nano-Zn-Mg-Mn-Fe composite: chemical and physical properties. *(A)* X-ray diffraction (XRD) pattern of the nano-Zn-Mg-Mn-Fe composite, showing distinct peaks that correspond to the crystalline phases within the composite material. The labelled peaks indicate the diffraction angles (2θ) associated with various crystal planes. *(B)* Fourier Transform Infrared (FTIR) spectra of the nano-Zn-Mg-Mn-Fe composite, along with the spectra of the individual salts used in its synthesis ($Fe_2(SO_4)_3$, $MgSO_4$, $MnSO_4$, and $ZnSO_4$). The marked peaks highlight the characteristic vibrations of functional groups, allowing for the comparison between the composite and its salt precursors. *(C)* SEM-EDX elemental analysis of the nano-Zn-Mg-Mn-Fe composite, showing the elemental composition of Fe, Mg, Mn, and Zn, along with other trace elements and impurities. The pie chart shows the relative percentages of these elements, with their specific concentrations provided in mg/L. These results represent the elemental incorporation into the composite and do not imply the presence of pure metallic forms or the absence of oxides. The detailed elemental composition data is presented in the accompanying table within **Figure S6**.

X-Ray Diffraction (XRD) analysis

Figure 2 A shows the XRD pattern of the Nano-Zn-Mg-Mn-Fe composite and reveals distinct crystallographic features, with peak positions at specific 2θ angles, including 21.2°, 26.6°, 28.3°, 30.7°, 35.8°, 37.1°, 40.4°, 44.7°, 50.1°, 58.6°, 66.4°, and 73.6°. These peaks correspond to various crystal planes within the composite, indicating the presence of multiple phases and

distinct crystallographic structures. The intensity of these peaks reflects the relative abundance of each crystal plane, with higher intensity peaks suggesting more prevalent or highly diffracting planes. The sharpness of the peaks suggests a high degree of crystallinity, which indicates well-ordered atomic arrangements. Broad peaks or shoulders would suggest amorphous regions, but in this case, the sharp peaks dominate and imply a well-crystallized structure.

The XRD peaks were analysed in detail to infer the possible phases present. The peaks at 21.2°, 26.6°, and 28.3° correspond to larger interplanar spacings, which indicate the presence of metal oxides such as ZnO and MgO. These materials are known for their hexagonal and cubical structures, respectively. The mid-range peaks at 30.7°, 35.8°, and 37.1° suggest smaller interplanar spacings, which correspond to more complex structures, including MnO_2 and Fe_2O_3 (Iron (III) oxide), both of which are common phases in such nanocomposites. Peaks at 40.4° and 44.7° often correspond to dense metal oxide structures, with the latter peak being characteristic of Fe_3O_4 (magnetite), which has an inverse spinel structure. Finally, the high-angle peaks at 50.1°, 58.6°, 66.4°, and 73.6° indicate the presence of small interplanar spacings, suggesting densely packed crystal planes. These peaks further support the presence of ZnO, MgO, and potentially a combination of metal oxides.

Based on these observations, several metal oxides phases could be identified in the composite. ZnO is confirmed by peaks at 21.2°, 26.6°, 28.3°, 40.4°, and 50.1°, indicating a hexagonal wurtzite structure. MgO contributes to the peaks at 21.2° and 26.6° with its cubic crystal structure. MnO_2 is identified by the peak at 35.8°, suggesting α-MnO_2 or β-MnO_2 polymorphs. Fe_2O_3 is indicated by the peak at 37.1°, consistent with the rhombohedral hematite structure, while Fe_3O_4 is suggested by the peak at 44.7°, confirming its inverse spinel structure. Together, these observations demonstrate that the nanocomposite consists of a combination of metal oxides, with a well-defined crystalline structure and multiple distinct phases.

Fourier Transform Infrared (FTIR) Spectroscopy

The FTIR spectra in Figure 2 B provides important insight into the chemical structure of the nano-Zn-Mg-Mn-Fe composite, particularly for its potential role in enhancing photosynthesis and UV protection in plants. Notable peaks at 3323 cm^{-1} and 1635 cm^{-1} correspond to O-H stretching and H-O-H bending, respectively, indicating hydroxyl groups that may aid in moisture retention and improve plant water absorption. The peak at 667 cm^{-1} is associated with metal-oxygen (M-O) stretching, confirming the formation of metal oxide bonds that are crucial for UV absorption and light utilization in photosynthesis.

Compared to the precursor salts $Fe_2(SO_4)_3$, $MgSO_4$, $MnSO_4$, and $ZnSO_4$, the composite shows shifted and broadened metal-oxygen peaks, suggesting strong chemical bonding between Zn, Mg, Mn, Fe, and O. Specifically, the Zn-O bond, observed at 1636 cm^{-1}, is critical for UV protection due to zinc oxide's known UV absorption properties, potentially enhancing plant resistance to UV stress. The Mn-O and Fe-O bonds at 371 cm^{-1} and 667 cm^{-1}, respectively, are important given the roles of manganese and iron in photosynthesis—manganese is involved in oxygen evolution, while iron is essential for chlorophyll synthesis and electron transport.(23,24) The Mg-O bonds further support the potential of the composite to enhance photosynthesis, as magnesium plays a pivotal role in chlorophyll function. In the chlorophyll molecule, magnesium exists as the central atom in the form of Mg^{2+}, coordinating with the porphyrin ring to facilitate light absorption and energy transfer essential for photosynthesis.

Elemental composition of the nano-Zn-Mg-Mn-Fe composite

The elemental composition of the synthesized nano-Zn-Mg-Mn-Fe composite was determined using SEM EDX analysis (Figure 2C). The results revealed magnesium as the most abundant element, comprising 26.75% of the total elemental distribution, followed by zinc (21.01%), iron (14.12%), and manganese (13.49%). Trace elements such as sodium, sulfur, chlorine, and

potassium were also detected, likely introduced during synthesis—particularly potassium from the KOH used as the precipitating agent. Minor variations in elemental proportions were observed compared to the initial stoichiometric precursor ratio of 2:1:1:1 (Zn:Mg:Fe:Mn), likely due to differences in incorporation efficiency during co-precipitation. These elemental percentages are used for discussion in the main text, while complementary data expressed in solution concentrations (mg/L) and nanoparticle-normalized values (mg/mg nanoparticle) are provided in the supplementary material (Figure S6) for reference. The relatively higher presence of magnesium and zinc may contribute to the enhanced functional performance of the nanocomposite, particularly in ultraviolet shielding and stress mitigation.

UV absorption and fluorescence properties for protection and upconversion

Figure 3 presents the UV-Vis absorption and fluorescence emission data for both the ionic mixture and nano-Zn-Mg-Mn-Fe composite at 100, 200, 300, and 500 mg/L (Figures 3A, 3B). In Figure 3A, the ionic mixture shows a progressive increase in absorbance as the concentration increases from 100 to 500 mg/L across the UV-visible range (200-500 nm). This suggests that the ionic form of the composite has significant UV absorption capabilities, particularly in the UV-C and UV-B regions, which are critical for sunscreen applications. Conversely, the nano-Zn-Mg-Mn-Fe composite (Figure 3B) shows relatively low absorbance across the same wavelength range, suggesting a reduced ability to absorb UV radiation directly when compared to the ionic mixture. This discrepancy could be attributed to particle aggregation or surface passivation of the nanoparticles in the composite, which may reduce the effective surface area for UV absorption.

However, despite the lower absorbance observed in the nanocomposite, the emission spectra (Figures 3C and 3D) show a distinct enhancement in the composite's fluorescence intensity compared to the ionic mixture. When excited at 300 nm (in the UV-B region), the

nanocomposite demonstrates strong emission peaks across the visible range, particularly between 400 nm and 600 nm. This higher fluorescence emission from the composite compared to the ionic mixture could be explained by a combination of factors. First, despite lower UV absorption, the nanocomposite may more effectively convert UV radiation (particularly UV-B) into visible light.(36) This conversion would help protect the plants by reducing the intensity of harmful UV rays reaching the plant surface and potentially enhances photosynthesis by making use of the converted light. Second, the nanocomposite may facilitate more efficient energy transfer mechanisms within its structure, allowing for greater radiative decay (fluorescence) despite low UV-Vis absorbance.(37) This suggests that the composite's structure promotes internal energy redistribution that favors emission over absorption. Third, the presence of metallic components such as Zn and Mn in the nanocomposite could contribute to localized Surface Plasmon Resonance **(**SPR) effects, which enhance fluorescence by amplifying local electromagnetic fields around the nanoparticles.(38) Last, the nanocomposite may possess a higher fluorescence quantum yield than its ionic counterparts, allowing it to convert absorbed light more efficiently into emitted light. (39) This would explain why it emits stronger fluorescence even with less UV absorption.

The strong fluorescence observed in the nano-Zn-Mg-Mn-Fe composite highlights significant potential as a multifunctional material for plant UV protection application. Although there is lower direct UV absorbance, the composite's ability to convert UV radiation into visible light

through fluorescence could serve as an effective protective mechanism by redirecting harmful UV energy away from the plant leaf surface.

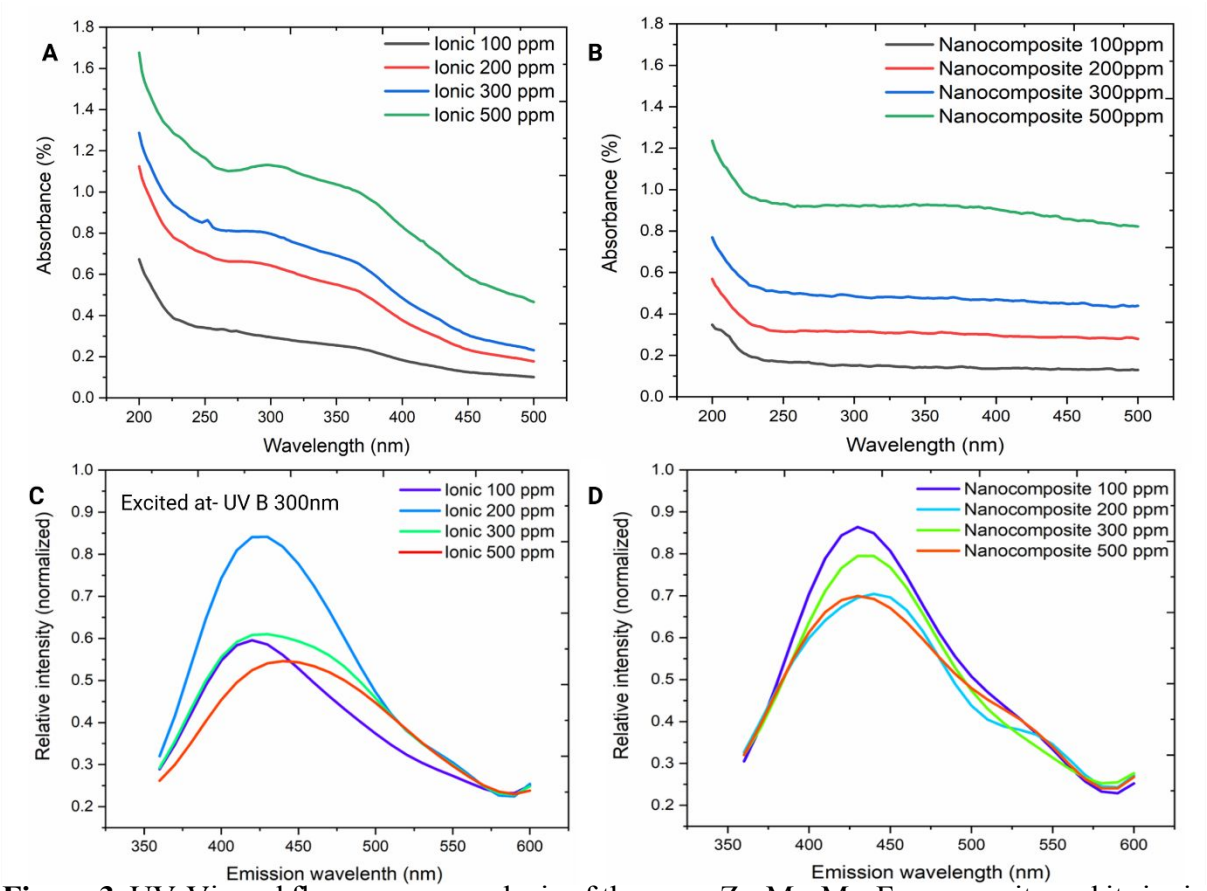

Figure 3. UV-Vis and fluorescence analysis of the nano-Zn-Mg-Mn-Fe composite and its ionic mixture. *(A)* UV-Vis absorption spectra of the ionic mixture at concentrations of 100, 200, 300, and 500 mg/L (ppm), showing the variation in absorbance with increasing concentration across the UV-visible range. *(B)* UV-Vis absorption spectra of the nano-Zn-Mg-Mn-Fe composite at concentrations of 100, 200, 300, and 500 mg/L (ppm), highlighting the composite's ability to absorb UV light in comparison to the ionic mixture. *(C)* Fluorescence emission spectra of the ionic mixture at concentrations of 100, 200, 300, and 500 mg/L (ppm), excited at 300 nm (UV-B region), illustrating the fluorescence intensity across emission wavelengths. *(D)* Fluorescence emission spectra of the nano-Zn-Mg-Mn-Fe composite at concentrations of 100, 200, 300, and 500 mg/L (ppm), excited at 300 nm (UV-B region), showing the fluorescence properties of the composite in response to UV-B excitation.

In vitro ionic release profile of the nano-Zn-Mg-Mn-Fe composite

The release and uptake kinetics of the nano-Zn-Mg-Mn-Fe composite were analysed both *in vitro* and *in planta* under standard LED lighting conditions. The *in vitro* study (Figure 4A) was conducted at 1000 mg/L of the nanocomposite, and monitored the release of elements from 15

min to 30 d. Based on the elemental composition of the nanocomposite, the initial concentrations of each element in the 1000 mg/L solution were as follows: Mn and Zn at 326.2 mg/L each, Fe at 239.5 mg/L, and Mg at 108.1 mg/L. Among these, magnesium exhibited the highest release rate, starting at approximately 70 mg/L at 15-min and gradually increasing to approximately 80 mg/L by 30 d, achieving nearly 74% release. Conversely, Zn, Mn, and Fe showed significantly lower release rates, with all three elements remaining below 10 mg/L throughout the study, releasing less than 3% of their total content. The stronger binding of Zn, Mn, and Fe within the composite matrix, as indicated by XRD and FTIR data, likely accounts for their slower diffusion into the solution. The controlled release patterns observed for Mn and Fe, characterized by low and steady increases over time, suggest a prolonged availability, which could be advantageous for sustained nutrient delivery and plant health.

In planta uptake dynamics of the nano-Zn-Mg-Mn-Fe composite and Ionic mixture

An *in planta* uptake study (Figure 4B) was conducted using a single concentration of 300 mg/L, applied as a foliar spray, to evaluate the absorption and translocation of elements from the nanocomposite over a four-day period. Among the tested elements, magnesium exhibited the highest uptake, increasing from approximately 180 mg/kg dry weight on Day 1 to over 220 mg/kg by Day 4. This reflects the high solubility and mobility of Mg within the plant system, consistent with its release profile observed in the *in vitro* dissolution study. The elevated Mg accumulation is likely due to the plant's higher physiological demand for magnesium and efficient uptake and storage mechanisms, especially during early stages of development.(27) In contrast, Zn, Mn, and Fe showed lower uptake levels, ranging between 40 and 60 mg/kg, with only moderate increases over time. These elements, while present in lower concentrations, appeared to follow a more gradual and sustained release pattern, potentially regulated by both the composite's release kinetics and the plant’s selective absorption mechanisms.(40)

To better understand the uptake dynamics, a comparative evaluation between the nanocomposite and ionic formulations was conducted based on additional nutrient uptake experiments, which are discussed later in the Results section. Despite being applied at equivalent elemental ratios, the ionic mixture demonstrated faster initial uptake, particularly for Zn and Fe, with concentrations peaking around 160–180 mg/kg dry weight in leaves within the first 24 hours. This rapid response is attributed to the immediate solubility of ionic forms, allowing direct absorption through the leaf surface. However, this quick uptake is often accompanied by rapid depletion due to leaching or redistribution within the plant, potentially limiting its long-term effectiveness.

On the other hand, the nanocomposite showed a slower, more controlled release profile, likely due to the incorporation of metal ions within the ferrite matrix structure. This gradual dissolution supports sustained nutrient availability and prolonged retention in plant tissues. Notably, root analysis revealed that ionic treatments led to greater Fe and Zn translocation to the aerial parts, whereas the nanocomposite facilitated higher Mn and Fe accumulation in roots, indicating localized delivery and retention. These differences underscore the distinct roles of ionic and nanocomposite formulations: while ionic forms may be more suitable for rapid, short-term nutrient supplementation, nanocomposites provide a more stable, long-term delivery system beneficial under prolonged stress conditions such as ultraviolet exposure. These findings highlight the importance of selecting delivery strategies tailored to plant growth stages and environmental needs. The observed uptake patterns are also influenced by factors such as leaf surface chemistry and particle transformation at the foliar interface—mechanisms that remain insufficiently understood and warrant further investigation.

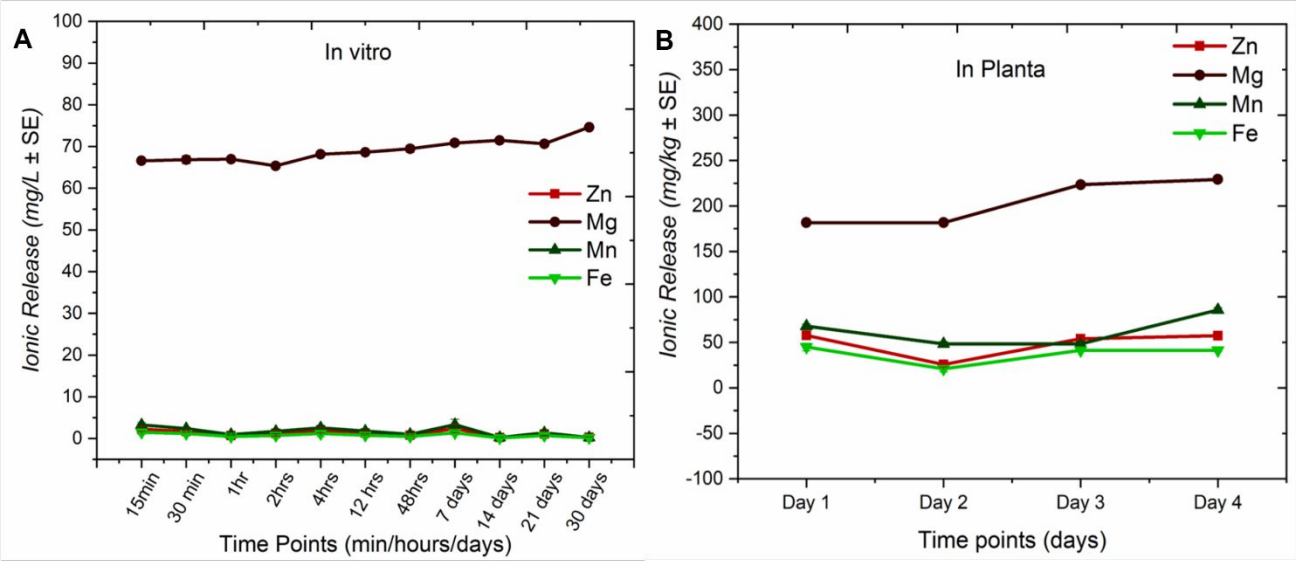

Figure 4. Ionic release and uptake kinetics of the nano-Zn-Mg-Mn-Fe composite as measured by ICP-OES over time in vitro and in planta. *(A)* In vitro ionic release profile measured at specific time intervals ranging from 15 minutes to 30 days. The graph shows the release of Zn, Mg, Mn, and Fe in parts per million (mg/L for in vitro measurements or mg/kg dry weight for in planta measurements), with error bars representing the standard error of the mean (n = 3). *(B)* In planta ionic release and uptake profile measured over four days, showing the accumulation of each element in the plant system from day 1 to day 4, expressed as mg/kg dry weight.

Assessment of UV protective effects on lettuce

Lettuce plants were exposed to high-intensity UV radiation (regular light regime + UV radiation) under various treatment conditions, including control (untreated), ionic Zn-Mg-Mn-Fe (abbreviated as "i") and nano-Zn-Mg-Mn-Fe composite (abbreviated as "n") treatments, each applied at concentrations of 100, 200, and 300 mg/L. The heatmap (Figure 5H) (41) illustrates the severity of UV damage across the treatments (Figure 5 A-G). UV damage scores were assigned using a defined rating scale (0–5) based on visible symptoms such as photobleaching, necrosis, and leaf deformation. Each plant was evaluated by blinded assessors, and categorical scores were compiled across treatment groups (n = 10 per treatment). Using OriginPro 8, the frequency of plants within each damage category (e.g., mild, moderate, severe) was calculated and visualized as a heatmap. Each cell in the heatmap represents the number of plants that exhibited a specific severity level for a given treatment, with colors ranging from

green (low severity) to red (high severity). For example, in the 300 mg/L nanocomposite group, most plants scored between 0 and 2 (mild damage), resulting in green cells, whereas the ionic 300 mg/L and control groups had more frequent scores of 4 or 5 (severe damage), leading to deep red cells. Representative images for each score category are shown in Figure 5BB to provide morphological context and support the visual scoring. Quantitative analysis showed that total UV damage severity scores were highest in the control (26 ± 1.03 SE) and ionic 300 mg/L (26 ± 0.55 SE) groups. In contrast, nanocomposite 300 mg/L treatment resulted in the lowest damage score (7 ± 0.73 SE), indicating superior protective performance. Intermediate levels of severity were observed in other treatment groups: Ionic 100 mg/L (12 ± 0.55 SE), Ionic 200 mg/L (14 ± 0.53 SE), nanocomposite 100 mg/L (15 ± 0.55 SE), and nanocomposite 200 mg/L (12 ± 0.55 SE). The experiment was conducted using a randomized block design, and all scoring was performed in a blinded manner to minimize bias.

The data demonstrate that environmentally relevant UV exposure (360–400 nm for 10 hours daily) induces significant stress in lettuce plants, with the severity of damage varying based on the type and concentration of the treatment applied. The untreated control group and the ionic 300 mg/L treatment both recorded the highest UV damage scores (26), exhibiting severe symptoms such as leaf necrosis, burning, and extensive yellowing. This indicates that the highest ionic concentration failed to provide protective effects. The lack of protection at 300 mg/L is likely due to ionic toxicity or osmotic stress, where excess free ions on the leaf surface exacerbate oxidative damage under UV rather than mitigate it. Importantly, plants treated with the same 300 mg/L ionic solution but exposed only to LED light showed no visible stress symptoms, confirming that the observed damage was UV-specific and not caused by the treatment itself. This highlights the importance of optimizing ionic concentrations, as over-application can diminish physiological resilience under environmental stress.

Conversely, nanocomposite-300 mg/L yielded the lowest damage score (7), suggesting that nanocomposite offered a "sunscreen" effect by reducing UV penetration into plant tissues and promoting stress tolerance. The differential response between ionic and nano treatments could be attributed to distinct mechanisms beyond the "sunscreen" effect, including how nanoparticles interact with plant cells. Nanoparticles are known to improve nutrient delivery and could potentially activate defence pathways in plants, enhancing their resilience to environmental stressors, including UV radiation.(42) Conversely, ionic treatments, particularly at higher concentrations, may disrupt cellular processes or lead to nutrient imbalances, exacerbating UV-induced damage. Additionally, the yellowing observed in most control and ionic-treated plants could be due to UV-induced chlorophyll degradation, a common symptom of photobleaching. The nano-treated plants, especially at 300 mg/L, showed less yellowing, indicating that the composite may help in protecting chlorophyll content, thereby maintaining photosynthetic efficiency under UV stress.

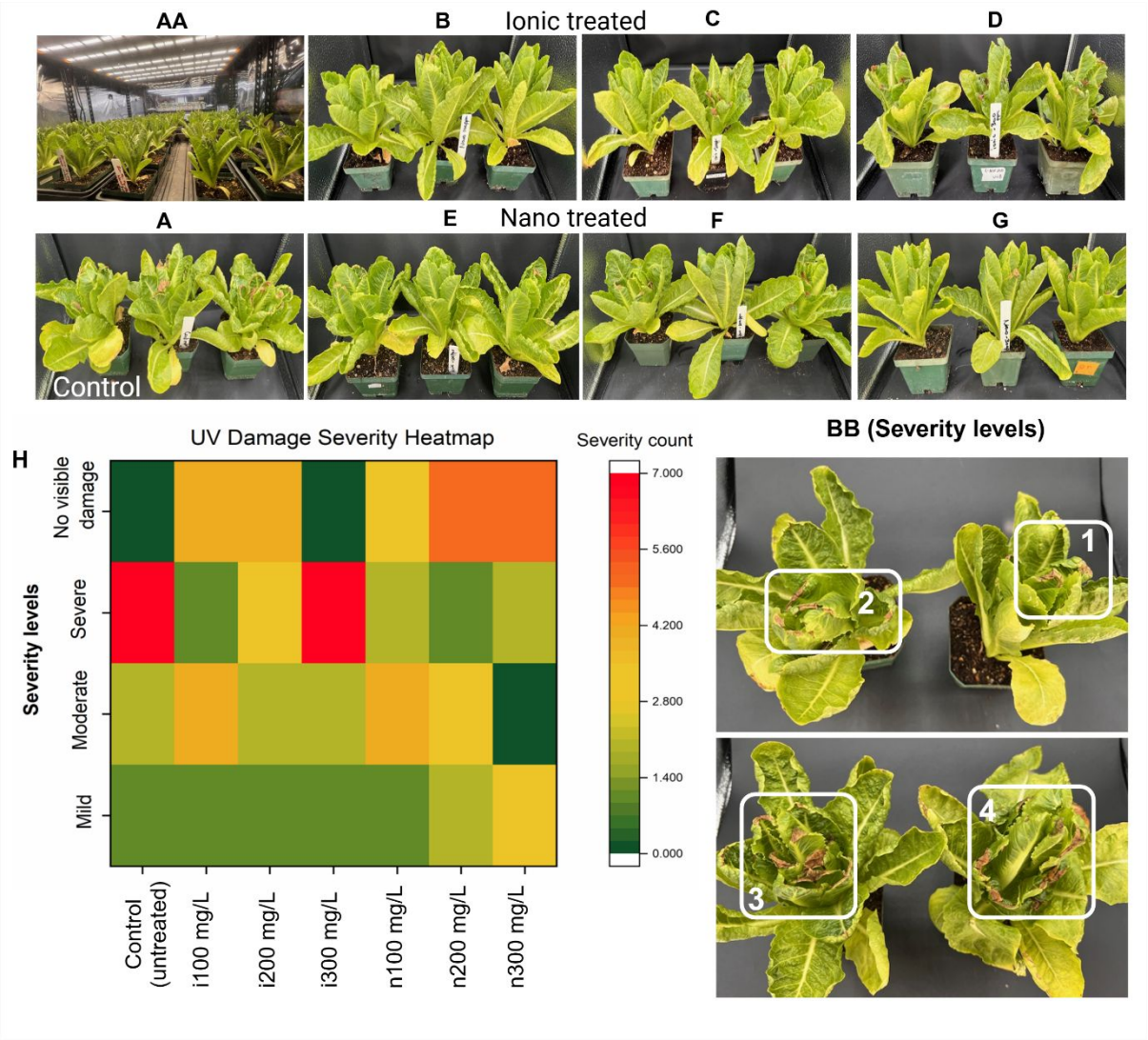

Figure 5. Lettuce plants exposed to UV radiation were evaluated for damage under different treatment conditions. **(AA)** shows lettuce plants growing under UV and light exposure, with **i** representing ionic treatments and **n** representing nanocomposite treatments *(A)* Control (mock-treated with water), *(B-D)* Ionic mixture treatments at concentrations of i100, i200, and i300 mg/L, and *(E-G)* Nano-Zn-Mg-Mn-Fe composite-treated at concentrations of n100, n200, and n300 mg/L. *(H)* Heatmap displaying the UV damage severity levels across different treatments. Each cell represents the number of instances for each severity level (Mild, Moderate, Severe, and No Visible Damage) for a particular treatment (n=10). The color scale ranges from 0.0 (none or mild, green) to 7.0 (high severity, red). *(BB)* Lettuce images illustrating different severity levels: 1. Mild burning symptoms, 2. Moderate yellowing, 3. Severe symptoms, and 4. Severe symptoms with yellowing. Most control and ionic-treated plants exhibited noticeable yellowing symptoms. The total scores across the treatments, starting from water-treated (control), ionic-treated, and nano-treated, are as follows: 26 for the control, 12 for ionic-100 mg/L, 14 for ionic-200 mg/L, 26 for ionic-300 mg/L, 15 for nanocomposite-100 mg/L, 12 for nanocomposite -200 mg/L, and 7 for nanocomposite -300 mg/L. The complete morphological effects of the lettuce plants under the entire set of treatments are shown in **Figure S5**.

Assessment of Plant Growth Under LED and UV

Under a regular LED lighting regime of 10 hours per day (Figure 6A), lettuce plants treated with various concentrations of the nanocomposite or ionic mixture showed significant improvements in growth parameters compared to the untreated control (Ctrl). Notable enhancements were observed in plant height (cm), leaf surface area (cm^2), number of leaves, root length (cm), and fresh biomass (g). These results indicate that both treatment types, particularly at higher concentrations, positively influenced vegetative growth under controlled lighting conditions. The improvements were concentration-dependent, with the highest increases in growth parameters seen at n300 mg/L, regardless of treatment. Significant increases in root length and fresh biomass were observed at n200 and n300 treatments ($*p < 0.001$). In Figure 6 B, the box plot shows a steady increase in dry biomass with increasing concentrations of the nano-composite treatment. Dry biomass increased significantly in all treatment groups compared to the untreated control. Specifically, the ionic treatments resulted in increases of 50.29% with i100, 38.44% with i200, and 30.00% with i300, while the nanocomposite treatments showed increases of 46.59% with n100, 26.27% with n200, and 72.63% with n300. All values are expressed as percentages relative to the control group, and the differences were statistically significant ($*p < 0.001$). This highlights the nutritional benefits of both treatments, with the nanocomposite showing the greatest improvement at the 300 mg/L concentration. Under UV light stress, the lettuce still showed positive responses to nanocomposite treatments (Figure 6 C). Increases in plant height, leaf surface area, number of leaves, root length, and fresh biomass were noted, with n300 treatment yielding the most significant improvements. In addition, root length and fresh biomass were substantially increased with n200 and n300 ($*p < 0.001$), demonstrating the nanocomposite's capability to alleviate UV stress and damage. The dry total biomass results (Figure 6 D) align with those of

the fresh weight data; n300 increased dry mass by 43.68%, while n200 and n100 resulted in 15.74% and 12.50% increases, respectively (*p < 0.001), compared to untreated control.

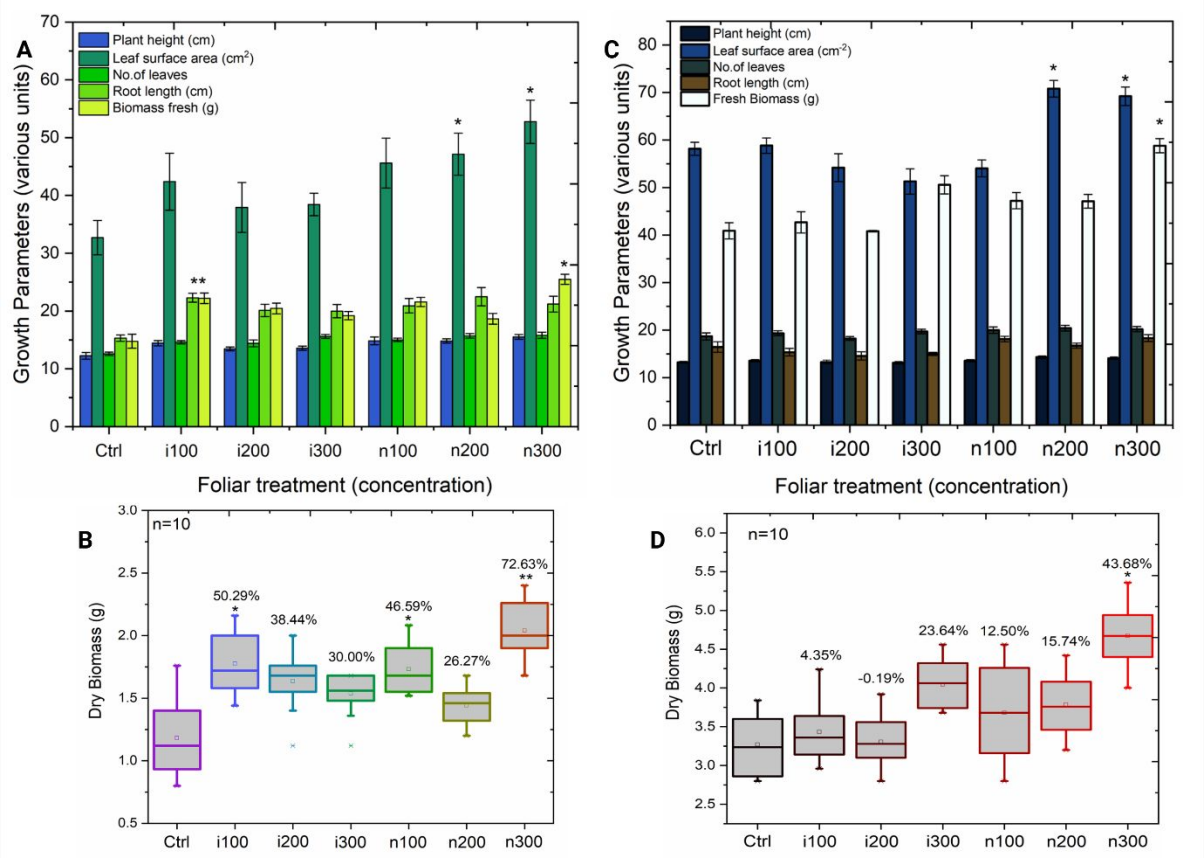

Figure 6. Effects of Nano-Zn-Mg-Mn-Fe composite and ionic mixture foliar treatments on the growth of lettuce plants exposed a regular light regime (LEDs as light source) and a regime including UV exposure. *(A)* Lettuce plants exposed to LED light were harvested and measured for plant height, leaf surface area, number of leaves, root length, and fresh biomass. Data represent the mean ± SE, with statistical significance indicated by *p < 0.001 and **p < 0.005. *(B)* Box plot showing dry biomass of lettuce plants under LED light. Data were analysed using one-way ANOVA with Tukey's test, indicating percentage (g) change compared to the control. *p < 0.001. *(C)* Lettuce plants exposed to LED+UV radiation was harvested and measured for plant height (cm), leaf surface area (cm^2), number of leaves, root length (cm), and fresh biomass (g). Data represent the mean ± SE, with statistical significance indicated by *p < 0.001. *(D)* Box plot showing dry biomass of lettuce plants under UV exposure. Data were analysed using one-way ANOVA with Tukey's test, showing percentage change compared to the control. *p < 0.001.

The foliar application of nano-Zn-Mg-Mn-Fe composites demonstrated a protective and growth-promoting effect on lettuce plants under UV stress conditions. UV light exposure typically generates reactive oxygen species (ROS), leading to oxidative stress, reduced growth,

and diminished productivity in plants.(11,43) However, the nano-composite treatments mitigated these negative effects, likely through the UV light conversion properties of the material. As evident in the fluorescence data, the nano-Zn-Mg-Mn-Fe composite can convert harmful UV radiation into less harmful visible light, reducing the intensity of UV radiation reaching the leaf surface, thus shielding the plants from direct UV damage. By acting as a UV filter, the nanocomposite allowed the plants to maintain robust physiological function under stress conditions, ultimately supporting greater health and biomass production. Additionally, the nanocomposite may have increased in planta antioxidant activity, particularly enzymatic defense such as superoxide dismutase (SOD), as shown below.

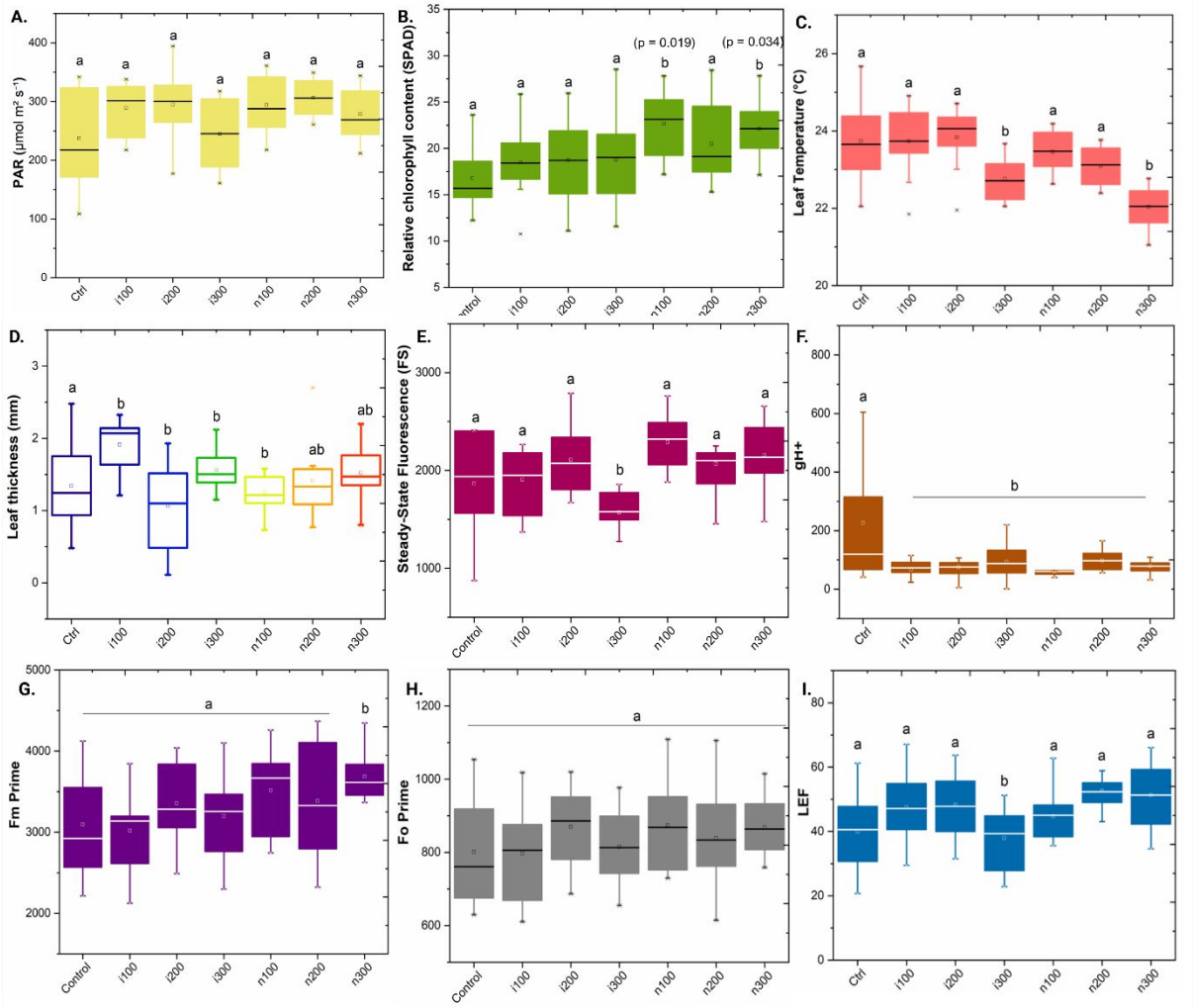

Figure 7. Photosynthetic parameters measured on lettuce plants after UV exposure and two weeks of post-treatment with the following: Control (no treatment), ionic mixture (100, 200, 300 mg/L), and Nano-Zn-Mg-Mn-Fe composite (100, 200, 300 mg/L). The parameters include:

(A) PAR (photosynthetically active radiation, light intensity), ***(B)*** Relative chlorophyll content (SPAD), ***(C)*** Leaf temperature (°C), ***(D)*** Leaf thickness (mm), ***(E)*** Steady-state fluorescence (FS), ***(F)*** gH+ (stomatal conductance), ***(G)*** Fm' (maximum fluorescence), ***(H)*** Fo' (minimal fluorescence), ***(I)*** LEF (linear electron flow). Different letters above the boxplots indicate statistically significant differences (Tukey's test, $p < 0.05$).

Photosynthetic response of lettuce to UV stress and nanocomposite treatment

The boxplots in **Figure 7** illustrate the positive impact of nano-Zn-Mg-Mn-Fe on several photosynthetic parameters in lettuce under UV stress compared to the control and ionic treatments. More specifically, both the ionic mixture and the nano-Zn-Mg-Mn-Fe composite treatments significantly influenced the photosynthetic parameters following UV exposure and during the two-week post-treatment recovery period. The nano-Zn-Mg-Mn-Fe composite treatments significantly improved Relative Chlorophyll Content (SPAD) (B), with increases of 33.3 and 66.7% at 100 and 300 mg/L, respectively, compared to the untreated control. Leaf Temperature (C) measurements displayed slight variations across treatments. While the ionic mixture treatments had no impact, the nanocomposites at 200 and 300 mg/L reduced leaf temperatures, likely contributing to protection against UV-induced heat stress. Leaf thickness (D) was significantly increased by the 100 mg/L ionic treatment, potentially indicating improved water retention or changes in leaf morphology as a protective adaptation to stress. In contrast, thinner leaves were observed across all other treatments, suggesting that higher concentrations may not always support beneficial structural traits under UV stress conditions. Steady-State Fluorescence (FS) (E) was increased with the nanocomposite at 100 mg/L compared to both the control and ionic treatments. This suggests enhanced photosynthetic efficiency and potential repair of photosystem II (PSII) under the influence of nanocomposites at low concentrations, while higher concentrations seemed to exhibit a neutral or slightly negative effect. The gH+ (F) represents stomatal conductance and showed high variability in the control group; however, significantly reduced stomatal activity was evident with all treatments, especially the nano-composited. This suggests that the treatments facilitate stomatal

regulation under UV stress, thereby optimizing water use efficiency. In terms of fluorescence parameters, FmPrime (G) was significantly enhanced with the nanocomposite at 100 mg/L, indicating improved PSII photochemical efficiency. However, higher concentrations of both the ionic mixture and nanocomposites did not exert further benefit, suggesting that lower concentrations are more effective for photosynthetic recovery after UV stress. LEF (I), or Linear Electron Flow, was enhanced by the nanocomposite at 100 and 200 mg/L, indicating improved electron transport through the photosystems, ensuring better energy conversion in the photosynthetic apparatus after UV-induced damage.

The results from this study suggest that the application of nanocomposites, particularly at 100 mg/L, positively impacts the recovery of photosynthetic processes in lettuce plants following UV stress. Significantly, the effects observed were concentration dependent. Lower concentrations (100 mg/L) consistently resulted in better recovery and photosynthetic efficiency, while higher concentrations (200-300 mg/L) had either neutral or even detrimental effects on leaf thickness and photosynthetic parameters. This aligns with previous studies indicating that excess metal ions or nanoparticles can disrupt plant homeostasis.(23,44) The enhanced chlorophyll content and decreased leaf temperature observed with the suggest conferred UV protection, potentially by acting as physical barriers to UV radiation and by stimulating oxidative stress pathways. The increased leaf thickness at 100 mg/L further supports this, as thicker leaves might indicate structural adaptation to environmental stress, aiding in water retention and mitigating UV damage. The reduction in stomatal conductance (gH+) across all treated nanocomposite groups suggests a possible role of the nanocomposites in regulating water loss under UV stress. This is crucial for plants under UV stress, as reduced stomatal conductance can help conserve water without severely affecting CO_2 uptake for photosynthesis.

Flavonoid and SOD activity in lettuce Under UV and nano-Treatment

Figure 8 presents the effects of UV exposure and post-treatment with the ionic or nano-Zn-Mg-Mn-Fe composite on total flavonoid content (Figure 8A) and superoxide dismutase (SOD) activity (Figure 8B). The highest total flavonoid content was with 300 mg/L of the ionic mixture, which was significantly greater than the untreated control and other treatments. Conversely, plants with the nano-Zn-Mg-Mn-Fe composite at 200 and 300 mg/L showed significantly reduced flavonoid content. The nanocomposite at 100 mg/L retained flavonoid levels comparable to the control. Superoxide dismutase (SOD) activity was significantly lower in plants treated with 300 mg/L of the nano-Zn-Mg-Mn-Fe composite compared to all other treatments, including the untreated control, clearly indicating decreased antioxidant enzyme activity at this concentration. The nanocomposite at 100 mg/L, as well as the ionic mixture at 200 and 300 mg/L, showed SOD activity similar to the untreated control.

These results highlight the differential effects of the ionic mixture and the nano-Zn-Mg-Mn-Fe composite on flavonoid content and antioxidant enzyme activity in lettuce under UV stress. Flavonoids are important secondary metabolites that serve as UV protectants and antioxidants in plants.(45) The significant increase in flavonoid content observed with the ions at 300 mg/L mitigation UV-induced oxidative damage. Conversely, the reduction in flavonoid content with nano-Zn-Mg-Mn-Fe composite treatment, especially at higher concentrations, suggests that the nanocomposite may provide sufficient UV protection, thus reducing the need for flavonoid accumulation as a defense response.(42) SOD is a key enzyme in the plant's defense system against reactive oxygen species (ROS), particularly under stress conditions like UV exposure.(42) Similarly, the observed decrease in SOD activity with higher concentrations of the nano-Zn-Mg-Mn-Fe composite may indicate that the composite itself reduces oxidative stress to a level where less enzymatic detoxification is required. This reduction in SOD activity could also suggest that the nanocomposite directly scavenges ROS or modulates ROS

production, thus reducing the burden on the plant's enzymatic antioxidant system. In contrast, the ionic mixture maintained or slightly enhanced SOD activity, indicating that it may not provide the same level of direct protection against ROS, requiring the plant to rely on endogenous antioxidant enzymes to manage oxidative stress. Collectively, these findings again demonstrate that the nanocomposite likely acts as both a physical shield against UV energy and enhances the plant's ability to cope with UV stress but impacting oxidative stress status without triggering secondary metabolite product.(46) It is also likely that the heterogeneous nanoparticle size and negative charge (-18 mV) may enhance their ability to adhere effectively to the plant surface, further enhancing UV-protective effects.

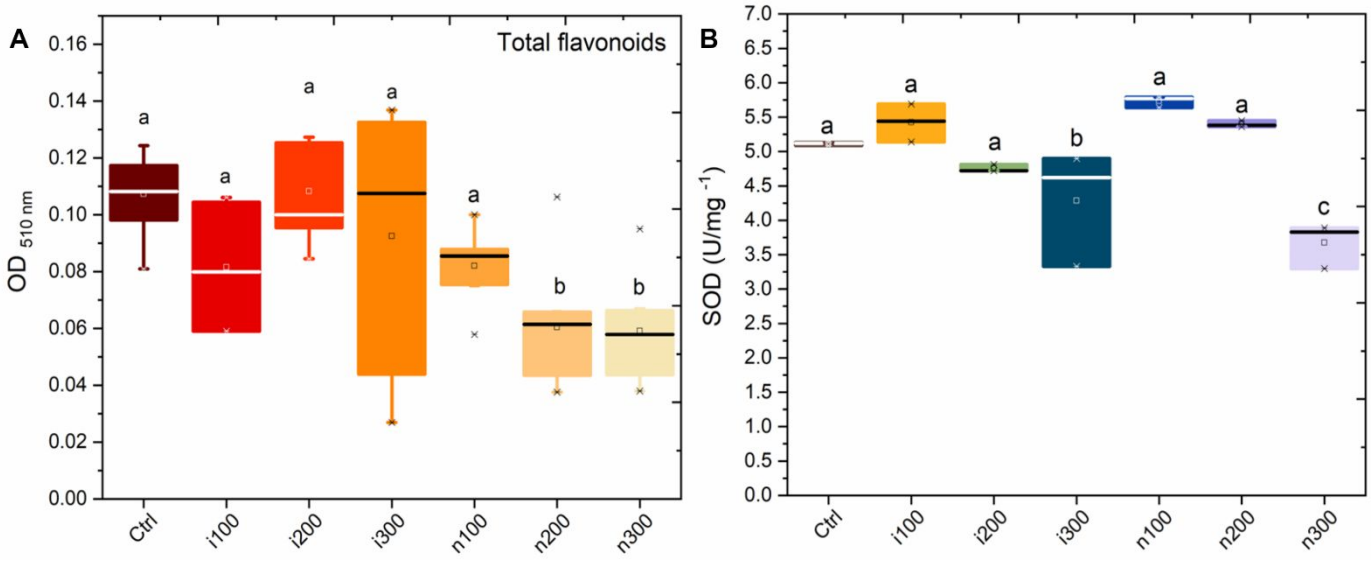

Figure 8. Total flavonoid content and SOD activity in lettuce plants after UV exposure and post two weeks of treatment with control (untreated), ionic mixture (100, 200, 300 mg/L), and Nano-Zn-Mg-Mn-Fe composite (100, 200, 300 mg/L). ***(A)*** Total flavonoid content was measured at OD 510 nm. The nano-Zn-Mg-Mn-Fe composite treatments (n100, n200, n300 mg/L) showed significantly lower flavonoid levels compared to the ionic mixtures (i100, i200, i300 mg/L), which had higher flavonoid content, particularly at 300 mg/L. ***(B)*** SOD activity was measured at OD 560 nm and expressed as U/mg. The nano-Zn-Mg-Mn-Fe composite at 300 mg/L (n300) resulted in significantly lower SOD activity compared to the control and other treatments, while the ionic mixture at 300 mg/L (i300) also exhibited a moderate decrease in SOD activity. Different letters indicate statistically significant differences (Tukey's test, $p < 0.05$).

Nutrient Dynamics in Lettuce Under LED and UV Exposure

The nutrient profile analysis of lettuce grown under LED exposure revealed distinct differences in nutrient accumulation patterns between plants treated with the ionic mixture and those treated with the nano Zn Mg Mn Fe composite (Figure S2A & B). Micronutrient uptake in lettuce is strongly influenced by environmental conditions such as light quality, substrate pH, and the chemical nature of nutrient formulations. Under controlled LED and UV exposure, differential uptake of magnesium, iron, zinc, and manganese was observed from both ionic and nanocomposite sources. A balanced supply of these micronutrients is essential to support photosynthesis, chlorophyll biosynthesis, and oxidative stress defense, particularly under high-light and UV stress conditions. The micronutrient concentrations observed in lettuce tissues were compared against published sufficiency ranges: Mg (2400–7300 ppm), Fe (150–250 ppm), Mn (55–110 ppm), and Zn (25–150 ppm), depending on cultivation method and plant stage.(47),(48) Fertility guidelines recommend maintaining substrate pH between 5.5 and 6.5 to optimize nutrient availability; for example, iron uptake becomes limited above pH 6.5, often resulting in interveinal chlorosis on upper leaves.

In our study, foliar application of the 300 mg/L ionic mixture significantly increased Zn concentration to 180 mg/kg dry weight, whereas the nanocomposite resulted in a moderate increase to 120 mg/kg dry weight. Mg levels remained stable across all treatments, ranging from 4,000 to 6,000 mg/kg dry weight, without significant differences from the control. Mn accumulation was most pronounced in leaves treated with the 300 mg/L nanocomposite, reaching 1,100 mg/kg dry weight, compared to minimal increases in other treatments. Similarly, Fe concentrations were enhanced with both the ionic mixture and nanocomposite at 300 mg/L, reaching around 200 mg/kg dry weight, highlighting their effectiveness in promoting Fe uptake in leaves.

In roots (Figure S2.B), the ionic mixture at 300 mg/L increased Zn concentration to 140 mg/kg dry weight, while the nanocomposite showed no significant effect on root Zn levels. Mg concentrations remained stable across treatments, ranging from 2,000 to 3,000 mg/kg dry weight. The nanocomposite demonstrated superior efficacy in Mn accumulation, increasing levels to 1,000 mg/kg dry weight at 300 mg/L, compared to minimal effects from the ionic mixture. Fe accumulation was highest in roots treated with the 300 mg/L nanocomposite, reaching 180 mg/kg dry weight, while the ionic mixture facilitated moderate increases, peaking at 120 mg/kg dry weight. These findings highlight the complementary nutrient delivery mechanisms of the ionic mixture, which enhanced Zn and Fe translocation to leaves, and the nanocomposite, which promoted sustained Mn and Fe retention in roots.

UV stress significantly impacted nutrient dynamics in lettuce compared to plants exposed to LED light, with ionic mixtures and nanocomposite treatments enhancing element uptake and translocation in a dose-dependent manner (Figure S3 A & B). In leaves (figure S3. A), Zn accumulation peaked at 300 mg/L of the ionic mixture (~160 mg/kg dry weight), while the nanocomposite resulted in moderate increases. Mg levels were highest with the 300 mg/L nanocomposite (~10,000 mg/kg dry weight) and the 200 mg/L ionic mixture (~9,000 mg/kg dry weight), reflecting improved uptake under stress. Mn showed significant increases in leaves with the 200 mg/L ionic mixture (~260 mg/kg dry weight), whereas the nanocomposite achieved moderate improvements. Fe concentrations were consistently elevated in leaves with the 200 and 300 mg/L ionic mixtures (~180 mg/kg dry weight) and the 200 mg/L nanocomposite (~150 mg/kg dry weight). The observed nutrient levels in roots may be influenced by the inherent nutrient content of the growth medium. Soil contributions, in conjunction with applied treatments, play a crucial role in nutrient availability and uptake. The interaction between nanocomposites (nanofertilizers)(49) and soil components can modify the bioavailability of nutrients, further affecting their accumulation in plant tissues. These factors

underscore the importance of considering both soil properties and fertilizer formulations in studies of plant nutrient dynamics.

In roots (figure S3. B), the nanocomposite at 100 mg/L significantly enhanced Zn accumulation (~150 mg/kg dry weight), while the ionic mixture showed minimal effect. Mg levels remained relatively stable across treatments, peaking at ~5,500 mg/kg dry weight with the 300 mg/L nanocomposite. Mn concentrations were substantially higher in roots treated with the 200 mg/L nanocomposite (~35 mg/kg dry weight), suggesting efficient delivery as intact nanoparticles. Fe levels increased in roots with the 300 mg/L nanocomposite (~180 mg/kg dry weight) and the 200 mg/L ionic mixture (~150 mg/kg dry weight), with the former indicating better retention. Fe concentrations were consistently elevated in both leaves and roots across all treatments. The ionic mixture promoted higher Fe accumulation in leaves, likely due to faster absorption, while the nanocomposite demonstrated better Fe retention in roots, indicating its potential for sustained delivery. The observed increase in Fe uptake under UV stress is particularly critical for maintaining redox balance and photosynthetic efficiency, underscoring the importance of these treatments in mitigating UV-induced stress.(23)

The differential effects of the ionic mixture and the nano-Zn-Mg-Mn-Fe composite on nutrient dynamics in lettuce highlight their unique nutrient delivery mechanisms. The ionic mixture facilitated rapid absorption of Zn and Fe, while the nanocomposite provided sustained release and efficient Mn translocation, particularly under UV stress conditions. Additionally, the role of the soil as a nutrient source contributed to elevated concentrations of certain elements, further influencing plant nutrient dynamics. These findings emphasize the potential of nano-based formulations to enhance nutrient management and improve plant resilience under variable environmental conditions.(50) An overall comparative summary of ionic vs. nanocomposite treatments on lettuce plants is provided in Table 2.

Table 2. Comparative Summary of Ionic vs Nanocomposite Treatments on Sprayed Lettuce Plants

Parameter	Ionic mixture (Zn-Mg-Mn-Fe) mg/L			Nanocomposite (Zn-Mg-Mn-Fe) mg/L		
	100	200	300	100	200	300
Chlorophyll Content	Moderate	High	Higher	High	Higher	Highest
Biomass (Dry weight)	↑	↑↑	↑↑↑	↑↑	↑↑↑	↑↑↑
UV damage score	18	15	12	10	8	6
Flavonoid content	Medium	Medium	Low	High	Very high	High
SOD activity	Normal	Medium	Low	High	High	Medium
Overall UV Protection	Medium	Better	Good	Good	Very good	Excellent
Mg uptake	+	+ +	+ + +	+ +	+ + +	+ + +
Fe uptake	+	+ +	+ +	+ +	+ + +	+ + +
Zn uptake	+	+ +	+ +	+ + +	+ + +	+ + + +
Mn uptake	+	+ +	+ +	+ + +	+ + +	+ + +

Conclusions

The nano-Zn-Mg-Mn-Fe composite exhibits strong potential as a multifunctional material in agricultural applications, particularly for providing UV protection and enhancing nutrient uptake in plants. Despite lower UV-Vis absorbance compared to the ionic mixture, the composite demonstrated superior fluorescence under UV-B excitation, effectively converting harmful UV radiation into useful visible light. This UV-conversion capability would not only shield plants from UV-induced stress but also facilitated photosynthesis, making the composite a promising candidate for mitigating the negative effects of UV exposure on crop growth.

The nano-Zn-Mg-Mn-Fe composite also improved the accumulation of key micronutrients (Mn, Mg and Fe), especially in the lettuce roots. At the highest concentration tested (300 mg/L), the composite provided sustained nutrient availability, while the ionic mixture promotes more immediate absorption, particularly of Zn, S, and K, making it effective for short-term nutrient enhancement. These findings suggest that nanocomposite may be more suitable for long-term nutrient management strategies due to their controlled release capabilities with anticipated UV stress, while ionic mixtures offer faster nutrient uptake.

The composite acts as a UV "sunscreen" for plants, reducing the need for stress-induced flavonoid production and SOD activity, allowing normal metabolic balance under UV stress. It also enhances K and Na accumulation under both LED and UV light, promoting stress tolerance and growth. The ionic mixture and nano-Zn-Mg-Mn-Fe composite highlight the need for tailored nutrient delivery based on specific crop needs and conditions. For stress marker reduction and UV protection, 300 mg/L was more effective, while 100 mg/L was better for promoting chlorophyll content and biomass. Optimizing the balance between short-term stress mitigation and long-term nutrient uptake is key. A dual-dose strategy, using 100 mg/L for early growth and 300 mg/L under heightened UV stress, offers an effective approach to maximize the composite's potential across varying scenarios.

Our future studies will explore the long-term effects of these treatments on plant health, growth, and productivity across different crops and under different UV exposure scenarios. Furthermore, we will assess the environmental and health implications of utilizing nanomaterials in agriculture, emphasizing green synthesis methods to reduce ecological risks and promote sustainability. For example, the feasibility of combining this material with nanocellulose as a substrate is currently being explored. The nanocellulose could act as a coating on plant leaves, providing an additional layer to enhance UV protection across various plant species, due to its film-forming properties and ability to create a protective barrier.

Collectively, the work demonstrates the significant potential on nano-enabled strategies to enhance crop resilience and promote yield in a changing climate.

Author contributions

R.M.T. led the project by designing the study, conducting the experiments, performing data analysis, and drafting the manuscript. **W.D.S** provided laboratory facilities and technical guidance for the plant experiments. **J.H.V**, **V.O.C**, and **J. L.G** contributed to manuscript drafting and critical review. **C.O.D** offered substantial support in experimental design, implementation, writing, reviewing, and editing. **J.W.** contributed significantly by providing key resources and strategic input. **N.Z.M** played a pivotal role in funding acquisition, co-designing the study, supporting experiment execution, and contributing to manuscript preparation. All authors actively contributed to refining and approving the final version of the manuscript.

Competing interests

The authors claim there are no competing interests.

Acknowledgement

Funding for this project was paid for by the U.S. Department of Agriculture's (USDA) Agricultural Marketing Service through grant 21SCBPCT1045. Its contents are solely the responsibility of the authors and do not necessarily represent the official views of the USDA. Funding was awarded and administered by the Connecticut Department of Agriculture.

References

1. Lowry GV, Giraldo JP, Steinmetz NF, Avellan A, Demirer GS, Ristroph KD, et al. Towards realizing nano-enabled precision delivery in plants. Nat Nanotechnol [Internet]. 2024 Jun 6; Available from: http://dx.doi.org/10.1038/s41565-024-01667-5

2. Bindraban PS, Dimkpa CO, Angle S, Rabbinge R. Unlocking the multiple public good services from balanced fertilizers. Food Secur [Internet]. 2018 Apr;10(2):273–85. Available from: http://dx.doi.org/10.1007/s12571-018-0769-4

3. Us Epa O. Health and environmental effects of ozone layer depletion. 2015 Jul 17 [cited 2024 Sep 20]; Available from: https://www.epa.gov/ozone-layer-protection/health-and-environmental-effects-ozone-layer-depletion

4. Heisler GM, Grant RH, Gao W, Slusser JR. Ultraviolet radiation and its impacts on agriculture and forests. Agric For Meteorol [Internet]. 2003 Dec;120(1–4):3–7. Available from: http://dx.doi.org/10.1016/j.agrformet.2003.08.007

5. Bernhard GH, Neale RE, Barnes PW, Neale PJ, Zepp RG, Wilson SR, et al. Environmental effects of stratospheric ozone depletion, UV radiation and interactions with climate change: UNEP Environmental Effects Assessment Panel, update 2019. Photochem

Photobiol Sci [Internet]. 2020 May 20;19(5):542–84. Available from: http://dx.doi.org/10.1039/d0pp90011g

6. Krupa SV, Kickert RN. The Greenhouse effect: impacts of ultraviolet-B (UV-B) radiation, carbon dioxide (CO2), and ozone (O3) on vegetation. Environ Pollut [Internet]. 1989;61(4):263–393. Available from: http://dx.doi.org/10.1016/0269-7491(89)90166-8

7. Gao W, Zheng Y, Slusser JR, Heisler GM, Grant RH, Xu J, et al. Effects of supplementary ultraviolet-B irradiance on maize yield and qualities: a field experiment. Photochem Photobiol [Internet]. 2004 Jul;80(1):127–31. Available from: http://dx.doi.org/10.1562/2004-05-03-RA-156.1

8. Xue S, Zang Y, Chen J, Shang S, Tang X. Effects of enhanced UV-B radiation on photosynthetic performance and non-photochemical quenching process of intertidal red macroalgae Neoporphyra haitanensis. Environ Exp Bot [Internet]. 2022 Jul;199(104888):104888. Available from: http://dx.doi.org/10.1016/j.envexpbot.2022.104888

9. Hollósy F. Effects of ultraviolet radiation on plant cells. Micron [Internet]. 2002;33(2):179–97. Available from: http://dx.doi.org/10.1016/s0968-4328(01)00011-7

10. Kataria S, Jajoo A, Guruprasad KN. Impact of increasing Ultraviolet-B (UV-B) radiation on photosynthetic processes. J Photochem Photobiol B [Internet]. 2014 Aug;137:55–66. Available from: http://dx.doi.org/10.1016/j.jphotobiol.2014.02.004

11. Shi C, Liu H. How plants protect themselves from ultraviolet-B radiation stress. Plant Physiol [Internet]. 2021 Nov 3;187(3):1096–103. Available from: http://dx.doi.org/10.1093/plphys/kiab245

12. Vanhaelewyn L, Van Der Straeten D, De Coninck B, Vandenbussche F. Ultraviolet radiation from a plant perspective: The plant-microorganism context. Front Plant Sci [Internet]. 2020 Dec 15;11:597642. Available from: http://dx.doi.org/10.3389/fpls.2020.597642

13. Qian M, Rosenqvist E, Prinsen E, Pescheck F, Flygare A-M, Kalbina I, et al. Downsizing in plants-UV light induces pronounced morphological changes in the absence of stress. Plant Physiol [Internet]. 2021 Sep 4;187(1):378–95. Available from: http://dx.doi.org/10.1093/plphys/kiab262

14. Ballaré CL, Barnes PW, Kendrick RE. Photomorphogenic effects of UV-B radiation on hypocotyl elongation in wild type and stable-phytochrome-deficient mutant seedlings of cucumber. Physiol Plant [Internet]. 1991 Dec;83(4):652–8. Available from: http://dx.doi.org/10.1111/j.1399-3054.1991.tb02483.x

15. Kalbin G, Hidema J, Brosché M, Kumagai T, Bornman JF, Strid Å. UV-B-induced DNA damage and expression of defence genes under UV-B stress: tissue-specific molecular marker analysis in leaves. Plant Cell Environ [Internet]. 2001 Sep;24(9):983–90. Available from: http://dx.doi.org/10.1046/j.1365-3040.2001.00748.x

16. Nazir M, Tungmunnithum D, Bose S, Drouet S, Garros L, Giglioli-Guivarc'h N, et al. Differential production of phenylpropanoid metabolites in callus cultures of Ocimum basilicum L. with distinct in vitro antioxidant activities and in vivo protective effects

against UV stress. J Agric Food Chem [Internet]. 2019 Feb 20;67(7):1847–59. Available from: http://dx.doi.org/10.1021/acs.jafc.8b05647

17. Wang F, Xu Z, Fan X, Zhou Q, Cao J, Ji G, et al. Transcriptome analysis reveals complex molecular mechanisms underlying UV tolerance of wheat (Triticum aestivum, L.). J Agric Food Chem [Internet]. 2019 Jan 16;67(2):563–77. Available from: http://dx.doi.org/10.1021/acs.jafc.8b05104

18. Jiang B, Geng F, Chang R, Ruan M, Bian Y, Xu L, et al. Comprehensive evaluation of the effect of ultraviolet stress on functional phytochemicals of hulless barley (qingke) grass in different growth times at vegetative stage. ACS Omega [Internet]. 2020 Dec 15;5(49):31810–20. Available from: http://dx.doi.org/10.1021/acsomega.0c04576

19. Hideg É, Strid Å. The effects of UV-B on the biochemistry and metabolism of plants. In: UV-B radiation and plant life: molecular biology to ecology [Internet]. UK: CABI; 2017. p. 90–110. Available from: http://dx.doi.org/10.1079/9781780648590.0090

20. Skibola CF, Smith MT. Potential health impacts of excessive flavonoid intake. Free Radic Biol Med [Internet]. 2000 Aug;29(3–4):375–83. Available from: http://dx.doi.org/10.1016/s0891-5849(00)00304-x

21. Vujovic M, Kostic E. Titanium dioxide and zinc oxide nanoparticles in sunscreens: A review of toxicological data. J Cosmet Sci [Internet]. 2019;70(5):223–34. Available from: https://www.ncbi.nlm.nih.gov/pubmed/31596227

22. Ruszkiewicz JA, Pinkas A, Ferrer B, Peres TV, Tsatsakis A, Aschner M. Neurotoxic effect of active ingredients in sunscreen products, a contemporary review. Toxicol Rep [Internet]. 2017 May 27;4:245–59. Available from: http://dx.doi.org/10.1016/j.toxrep.2017.05.006

23. Thangavelu RM, da Silva WL, Zuverza-Mena N, Dimkpa CO, White JC. Nano-sized metal oxide fertilizers for sustainable agriculture: balancing benefits, risks, and risk management strategies. Nanoscale [Internet]. 2024 Nov 7;16(43):19998–20026. Available from: http://dx.doi.org/10.1039/d4nr01354a

24. Alejandro S, Höller S, Meier B, Peiter E. Manganese in plants: From acquisition to subcellular allocation. Front Plant Sci [Internet]. 2020 Mar 26;11:300. Available from: http://dx.doi.org/10.3389/fpls.2020.00300

25. Therby-Vale R, Lacombe B, Rhee SY, Nussaume L, Rouached H. Mineral nutrient signaling controls photosynthesis: focus on iron deficiency-induced chlorosis. Trends Plant Sci [Internet]. 2022 May;27(5):502–9. Available from: http://dx.doi.org/10.1016/j.tplants.2021.11.005

26. Hamzah Saleem M, Usman K, Rizwan M, Al Jabri H, Alsafran M. Functions and strategies for enhancing zinc availability in plants for sustainable agriculture. Front Plant Sci [Internet]. 2022 Oct 7;13:1033092. Available from: http://dx.doi.org/10.3389/fpls.2022.1033092

27. Ishfaq M, Wang Y, Yan M, Wang Z, Wu L, Li C, et al. Physiological essence of magnesium in plants and its widespread deficiency in the farming system of China. Front

Plant Sci [Internet]. 2022 Apr 25;13:802274. Available from: http://dx.doi.org/10.3389/fpls.2022.802274

28. Jamali Jaghdani S, Jahns P, Tränkner M. The impact of magnesium deficiency on photosynthesis and photoprotection in Spinacia oleracea. Plant Stress [Internet]. 2021 Dec;2(100040):100040. Available from: http://dx.doi.org/10.1016/j.stress.2021.100040

29. Shoukat A, Pitann B, Zafar MM, Farooq MA, Haroon M, Nawaz A, et al. Nanotechnology for climate change mitigation: Enhancing plant resilience under stress environments. J Plant Nutr Soil Sci [Internet]. 2024 Oct;187(5):604–20. Available from: http://dx.doi.org/10.1002/jpln.202300295

30. Thakur A, Singh M. Preparation and characterization of nanosize Mn0.4Zn0.6 Fe2O4 ferrite by citrate precursor method. Ceram Int [Internet]. 2003 Jan;29(5):505–11. Available from: http://dx.doi.org/10.1016/s0272-8842(02)00194-3

31. [cited 2024 Dec 30]. Available from: https://openai.com

32. Version 2022"). OriginLab Corporation. In: Version Number. Northampton, MA, USA;

33. Cangussú LV de S, da Silva TP, Bertolazi AA, Batista PSC, de França VCPLA, Campos WF, et al. Combined effect of humic acids and Serendipita indica on photosynthesis and yield of bean plants. S Afr J Bot [Internet]. 2024 Dec;175:158–68. Available from: http://dx.doi.org/10.1016/j.sajb.2024.10.030

34. Iqbal A, Jacob J, Mahmood A, Mehboob K, Mahmood K, Ali A, et al. Synthesis and characterization of Zn–Mn–Fe nano oxide composites for the degradation of reactive yellow 15 dye. Physica B Condens Matter [Internet]. 2020 Jul;588(412210):412210. Available from: http://dx.doi.org/10.1016/j.physb.2020.412210

35. Abdel Azeem SM, Wahsh MMS, Youssef FH, Ibrahim AMH, Burham N. Magnetic nanocomposite of zinc–manganese ferrite/polyurethane foam for adsorption of copper and cadmium from water. Desalination Water Treat [Internet]. 2022 Aug;267:26–44. Available from: http://dx.doi.org/10.5004/dwt.2022.28643

36. Sasani Ghamsari M, Alamdari S, Han W, Park H-H. Impact of nanostructured thin ZnO film in ultraviolet protection. Int J Nanomedicine [Internet]. 2017;12:207–16. Available from: http://dx.doi.org/10.2147/IJN.S118637

37. Abebe B, Murthy HCA, Zereffa EA. Multifunctional application of PVA-aided Zn-Fe-Mn coupled oxide nanocomposite. Nanoscale Res Lett [Internet]. 2021 Jan 2;16(1):1. Available from: http://dx.doi.org/10.1186/s11671-020-03464-0

38. Marica I, Nekvapil F, Ștefan M, Farcău C, Falamaș A. Zinc oxide nanostructures for fluorescence and Raman signal enhancement: a review. Beilstein J Nanotechnol [Internet]. 2022 May 27;13:472–90. Available from: http://dx.doi.org/10.3762/bjnano.13.40

39. Chen G, Qiu H, Prasad PN, Chen X. Upconversion nanoparticles: design, nanochemistry, and applications in theranostics. Chem Rev [Internet]. 2014 May 28;114(10):5161–214. Available from: http://dx.doi.org/10.1021/cr400425h

40. Tighe-Neira R, Gonzalez-Villagra J, Nunes-Nesi A, Inostroza-Blancheteau C. Impact of nanoparticles and their ionic counterparts derived from heavy metals on the physiology of

food crops. Plant Physiol Biochem [Internet]. 2022 Feb 1;172:14–23. Available from: http://dx.doi.org/10.1016/j.plaphy.2021.12.036

41. Gupta SK, Sharma M, Deeba F, Pandey V. Plant response. In: UV-B Radiation [Internet]. Chichester, UK: John Wiley & Sons, Ltd; 2017. p. 217–58. Available from: http://dx.doi.org/10.1002/9781119143611.ch12

42. Soni S, Jha AB, Dubey RS, Sharma P. Application of nanoparticles for enhanced UV-B stress tolerance in plants. Plant Nano Biology [Internet]. 2022 Nov;2(100014):100014. Available from: http://dx.doi.org/10.1016/j.plana.2022.100014

43. Prasad SM, Dwivedi R, Zeeshan M. Growth, photosynthetic electron transport, and antioxidant responses of young soybean seedlings to simultaneous exposure of nickel and UV-B stress. Photosynthetica [Internet]. 2005 Jun 1;43(2):177–85. Available from: http://dx.doi.org/10.1007/s11099-005-0031-0

44. Wei L, Liu J, Jiang G. Nanoparticle-specific transformations dictate nanoparticle effects associated with plants and implications for nanotechnology use in agriculture. Nat Commun [Internet]. 2024 Aug 27;15(1):7389. Available from: http://dx.doi.org/10.1038/s41467-024-51741-8

45. Roy A, Khan A, Ahmad I, Alghamdi S, Rajab BS, Babalghith AO, et al. Flavonoids a bioactive compound from medicinal plants and its therapeutic applications. Biomed Res Int [Internet]. 2022 Jun 6;2022:5445291. Available from: http://dx.doi.org/10.1155/2022/5445291

46. Silva MRF, Alves MFRP, Cunha JPGQ, Costa JL, Silva CA, Fernandes MHV, et al. Nanostructured transparent solutions for UV-shielding: Recent developments and future challenges. Mater Today Phys [Internet]. 2023 Jun;35(101131):101131. Available from: http://dx.doi.org/10.1016/j.mtphys.2023.101131

47. Liu J, Roland Leatherwood W, Mattson NS. Irrigation method and fertilizer concentration differentially alter growth of vegetable transplants. Horttechnology [Internet]. 2012 Feb;22(1):56–63. Available from: http://dx.doi.org/10.21273/horttech.22.1.56

48. Mills HA, Bryson G. Plant Analysis Handbook IV [Internet]. Micro Macro Publishing; 2015. Available from: http://dx.doi.org/10.13140/2.1.1693.2646

49. Toksha B, Joshi S, Chatterjee A. The potential of nanocomposite fertilizers for sustainable crop production. In: Nanotechnology in the Life Sciences [Internet]. Cham: Springer Nature Switzerland; 2024. p. 99–124. Available from: http://dx.doi.org/10.1007/978-3-031-41329-2_4

50. Saurabh K, Prakash V, Dubey AK, Ghosh S, Kumari A, Sundaram PK, et al. Enhancing sustainability in agriculture with nanofertilizers. Discov Appl Sci [Internet]. 2024 Oct 20;6(11). Available from: http://dx.doi.org/10.1007/s42452-024-06267-5

51. ChatGPT [Internet]. [cited 2025 Apr 4]. Available from: https://chat.openai.com/

52. Wang M, Zheng Q, Shen Q, Guo S. The critical role of potassium in plant stress response. Int J Mol Sci [Internet]. 2013 Apr 2;14(4):7370–90. Available from: http://dx.doi.org/10.3390/ijms14047370

53. Khan F, Siddique AB, Shabala S, Zhou M, Zhao C. Phosphorus plays key roles in regulating plants' physiological responses to abiotic stresses. Plants [Internet]. 2023 Aug 3;12(15). Available from: http://dx.doi.org/10.3390/plants12152861

54. Li Q, Gao Y, Yang A. Sulfur homeostasis in plants. Int J Mol Sci [Internet]. 2020 Nov 25;21(23):8926. Available from: http://dx.doi.org/10.3390/ijms21238926

55. Noctor G, Mhamdi A, Chaouch S, Han Y, Neukermans J, Marquez-Garcia B, et al. Glutathione in plants: an integrated overview. Plant Cell Environ [Internet]. 2012 Feb;35(2):454–84. Available from: http://dx.doi.org/10.1111/j.1365-3040.2011.02400.x

56. Yamaguchi T, Hamamoto S, Uozumi N. Sodium transport system in plant cells. Front Plant Sci [Internet]. 2013 Oct 17;4:410. Available from: http://dx.doi.org/10.3389/fpls.2013.00410

Data Availability Statement

All data supporting the findings of this study are provided in the manuscript and supplementary information. Additional raw data will be made available upon reasonable request.